Diastereoselective synthesis and two-step photocleavage of ruthenium polypyridyl complexes bearing a bisthioether ligand

*Michael S. Meijer and Sylvestre Bonnet**

Leiden Institute of Chemistry, Leiden University, P.O. Box 9502, 2300 RA Leiden, The Netherlands.

*Corresponding author: *bonnet@chem.leidenuniv.nl*

SUPPORTING INFORMATION

1) Table of contents

2) Atom numbering schemes used for NMR attribution

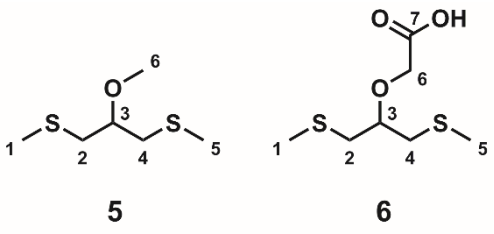

Scheme S1. Structural formulas of compounds 5, and 6, showing the atom numbering used in NMR attribution.

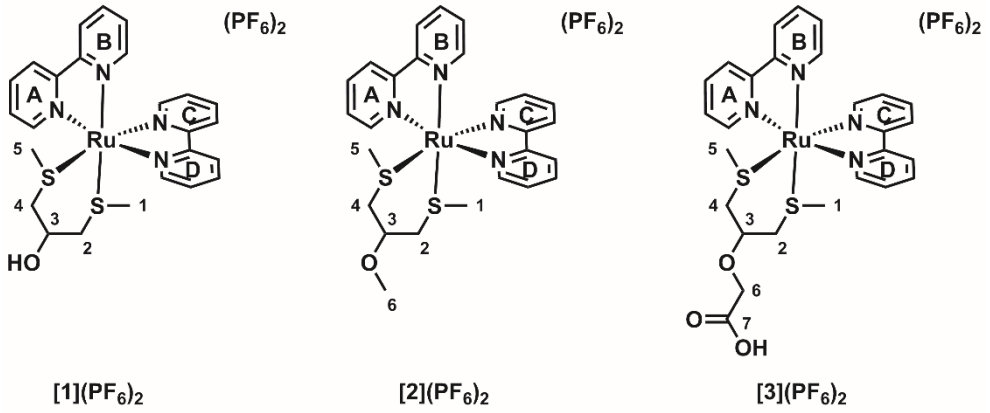

Scheme S2. Structural formulas of compounds [1](PF$_6$)$_2$, [2](PF$_6$)$_2$, and [3](PF$_6$)$_2$, showing the atom numbering used in NMR attribution.

3) Photosubstitution quantum yields of [1–3](PF$_6$)$_2$ under blue-light irradiation

Table S1. Conditions of the photoreactions monitored by UV-Vis absorption spectroscopy and MS.

Entry	Complex	Solvent	[Ru] / μM	λ_{exc} / nm	q_p / mol·s^{-1}	t / min
1	[**1**](PF$_6$)$_2$	H_2O	72	443	2.65×10^{-8}	120
2	[**2**](PF$_6$)$_2$	H_2O	181	443	2.85×10^{-8}	120
3	[**3**](PF$_6$)$_2$	H_2O	99	443	2.85×10^{-8}	120

Data treatment and quantum yield calculation: For a photosubstitution reaction in which a starting complex, **R**, is converted into a photoproduct, **P**, by the substitution of a ligand for one of more solvent molecules, the photosubstitution quantum yield, Φ_λ, can be directly calculated from the first-order photochemical rate constant, k_Φ, derived directly from a mono-exponential fit of the change to the UV-Vis absorption spectrum at a certain wavelength *versus* time, if the following conditions are met:

(a) both the reagent **R** and the photoproduct **P** are thermally stable, and have significantly different UV-Vis absorption spectra;
(b) the photosubstituted ligand and the incoming solvent molecule do not absorb light at the irradiation wavelength, nor at the fitted wavelength;
(c) the photochemical reaction is an (apparent) single step photoreaction;
(d) irradiation is performed at a wavelength near the isosbestic point of the photoreaction, i.e. where the absorbance of the solution is constant throughout the photoreaction.

Under these circumstances, k_Φ can be converted into the photosubstitution quantum yield, Φ_λ, using Equation S1:

$$\Phi_\lambda = \frac{k_\Phi \cdot n_{\mathbf{R}}}{q_p \cdot (1-10^{-A_\lambda})} \qquad \text{Equation (S1)}$$

where, k_Φ is the found photochemical rate constant, $n_{\mathbf{R}}$ is the amount of reagent at the start of the reaction, q_p is the incoming photon flux, and A_λ is the absorbance at the irradiation wavelength.

If the final condition (d) set above is not met, i.e. the irradiation is performed at a wavelength that is not an isosbestic point, the photosubstitution quantum yield can be calculated following a method discussed previously in detail by Bahreman and Bonnet.[1] Here, Φ_λ can be obtained from the slope of a plot of the number of mol of **R** ($n_{\mathbf{R}}$) *vs.* the total number of mol of photons absorbed by **R** ($Q_{i,\mathbf{R}}$) between $t = t_0$ and $t = t_i$. Thus, $Q_{i,\mathbf{R}}$ is calculated according to Equation S2:

$$Q_{i,\mathbf{R}}(t) = \sum_{t=0}^{i} q_{i,\mathbf{R}} \qquad \text{Equation (S2)}$$

where $q_{i,\mathbf{R}}$ is the moles of photons absorbed by **R** between two consecutive UV-Vis absorption measurements at t_{i+1} and t_i ($\Delta t = t_{i+1} - t_i$). Assuming that absorbance is constant in this time interval Δt, $q_{i,\mathbf{R}}$ can be calculated according to Equation S3:

$$q_{i,\mathbf{R}} = \left(\frac{(A_{\mathbf{R}})_{ave}}{(A_{tot})_{ave}}\right)_i \cdot (1 - 10^{-3\cdot(A_{tot})_{ave}}) \cdot q_p \cdot \Delta t \qquad \text{Equation (S3)}$$

where $(A_{\mathbf{R}})_{ave}$ is the average absorbance of **R** between two consecutive UV-Vis absorption measurements, $(A_{tot})_{ave}$ is the average total absorbance of the solution at the irradiation wavelength between the same consecutive UV-Vis absorption measurements, q_p is the photon flux of the irradiation source at the irradiation wavelength, and $(1 - 10^{-3 \cdot (A_{tot})_{ave}})$ is the probability of absorption of a photon. The multiplication factor 3 is necessary as irradiation is performed from the top of the 1.0 × 1.0 cm cuvette through 3 mL of solution, resulting in a 3 cm pathlength of irradiation, compared to a 1 cm pathlength for the measurement of absorbances (performed from the side of the cuvette).

The value of $n_{\mathbf{R}}$, and by extension $(A_{\mathbf{R}})_{ave}$, is typically calculated by the two-wavelength method, where the time evolution of the concentrations of the two absorbing species (**R** and **P**) is obtained by following the time evolution of the absorbance at two different wavelengths, using the molar extinction coefficients (ε) of the two species at these wavelengths.[1]

In this work, however, we discussed several sequential two-step photosubstitution reactions, following the general equation **R** → **I** → **P,** whereby both conditions (c) and (d) above are not met. As the intermediate species (**I**) in the photoreaction cannot be isolated and is thermally unstable, its molar extinction coefficients (ε) is not known. Thus, the two-wavelength method cannot be used to calculate the time evolution of the concentrations of species **R**, **I** and **P** in time.

In this case, we performed a global fitting of the time-dependent evolution of the UV-Vis absorption spectra, using the Glotaran software package.[2] Using this approach, we obtained both the fitted UV-Vis absorption spectra of species **R**, **I** and **P**, as well as the time-evolution of the relative concentrations (Figure S15B for the photosubstitution of [**1**](PF$_6$)$_2$ in water). Using the known molar extinction coefficients of the starting compound **R**, we calculated the molar extinction coefficients of **I** and **P** (Figure S15A), and the total concentration of ruthenium $n_{\mathbf{R},t=0}$. From the time evolution of the relative concentrations and the molar absorption coefficient of all species, we could derive the time evolution of $n_{\mathbf{R}}$, $n_{\mathbf{I}}$, and $n_{\mathbf{P}}$, as well as $Q_{i,\mathbf{R}}$ and $Q_{i,\mathbf{I}}$, the total number of mol of photons absorbed between $t = t_0$ and $t = t_i$ by **R** and **I**, respectively. The slope of the plot of $n_{\mathbf{R}}$ *vs.* $Q_{i,\mathbf{R}}$ (Figure S15C) gives the quantum yield of the first step of the reaction. Similarly, the slope of the plot of $n_{\mathbf{P}}$ *vs.* $Q_{i,\mathbf{I}}$ (Figure S15D) gives the quantum yield of the second step of the reaction.

Notably, in the global fitting performed using the Glotaran software package, we employed a sequential first-order kinetic model, which assumes that both reactions are first order reactions, i.e. only dependent of the concentration of the reacting species. This first-order approximation for photochemical reactions is only valid at wavelengths where the probability of absorbance does not change significantly over time, i.e. at the isosbestic point. As the reactions studied here are sequential two-step reactions, they have sequential, non-overlapping isosbestic points (Figure S15A), which prevents us from irradiating the solution at a point where the probability of absorbance does not change during both steps. Although the reactions studied here do therefore not strictly fulfil all the requirements for the application of a first-order kinetic model, we found that such a model fits the data well, as long as the molar extinction coefficients of the species involved are not too different at the irradiation wavelength. The slight deviation from linearity in Figure S15C and Figure S15D may be related to the use of this first-order approximation.

Kinetic data for the photosubstitution of [**2**](PF$_6$)$_2$ and [**3**](PF$_6$)$_2$ in water are shown in Figure S16 and Figure S17.

4) Singlet oxygen generation and phosphorescence quantum yield of [1–3](PF$_6$)$_2$

The quantum yields of singlet oxygen generation and phosphorescence were determined in a custom-built setup (Scheme S3). All optical parts were connected with optical fibres from Avantes, with a diameter of 200–600 µm. 500 µL of sample, consisting of the compound in deuterated methanol, was added to a 104F-OS semi-micro fluorescence cuvette from Hellma Analytics, and placed in a CUV-UV/VIS-TC temperature-controlled cuvette holder (Avantes). Temperature control was performed with the use of a TC-125 controller from Quantum Northwest. The sample was allowed to equilibrate at 298 K for 5 minutes. Emission spectroscopy was performed with a 450 nm fibre-coupled laser (LRD-0450, Laserglow), which was set to 50 mW at the cuvette (4 mm beam diameter; 0.4 W·cm^{-2}) at a 90° angle with respect to the spectrometer. The excitation power was measured using a S310C thermal sensor connected to a PM100USB power meter (Thorlabs). The emission spectra were recorded using two separate spectrometers for the UV-Vis and NIR emission, i.e. from 300 nm to 1000 nm for the phosphorescence of the complex (Avantes 2048L StarLine spectrometer) and from 1000 nm to 1700 nm for the phosphorescence of singlet oxygen ($^1\Delta_g$) around 1275 nm (Avantes NIR256-1.7TEC spectrometer, detector set to −12 °C). Both spectrometers were calibrated using an Avalight-HAL-CAL-ISP30 NIST traceable calibration lamp from Avantes directly before the measurement. The infrared emission spectrum was acquired within 9 seconds, after which the laser was turned off directly. Similarly, the visible emission spectrum was acquired within 2 seconds. UV-Vis absorption spectra before and after emission spectroscopy were measured using an Avalight-DHc halogen-deuterium lamp (Avantes) as light source (turned off during emission spectroscopy) and the before mentioned UV-Vis spectrometer as detector, both connected to the cuvette holder at a 180° angle. All spectra were recorded using Avasoft 8.5 software from Avantes and further processed using Microsoft Office Excel 2010 and Origin Pro 9.1 software.

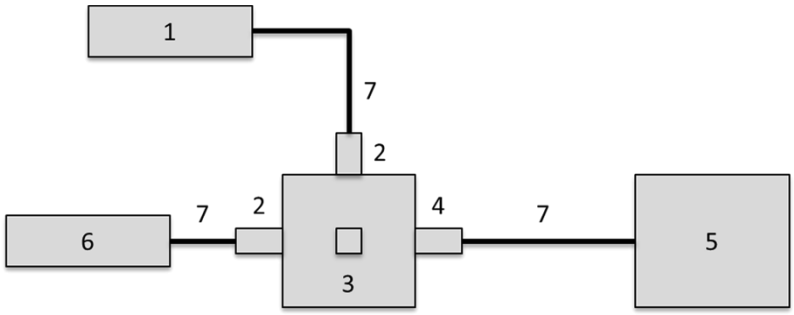

Scheme S3. Setup used for singlet oxygen generation and phosphorescence quantum yield experiments. (1) CW laser light source, (2) collimating lens, (3) temperature-controlled cuvette holder. (4) double collimator, (5) UV-Vis (300–1000 nm) or NIR (1000–1700 nm) CCD spectrometer, (6) UV-Vis halogen-deuterium light source, and (7) optical fibres.

The quantum yields of phosphorescence and singlet oxygen production was calculated using the relative method with [Ru(bpy)$_3$]Cl$_2$ as the standard (Φ_Δ = 0.73,[3, 4] Φ_P = 0.015 in CD$_3$OD), according to Equation S4. The phosphorescence quantum yield of [Ru(bpy)$_3$]Cl$_2$ in CD$_3$OD was determined by absolute methods (see below).

$$\Phi_{\mathrm{sam}} = \Phi_{\mathrm{std}} \times \frac{A_{\mathrm{std}}^{450}}{A_{\mathrm{sam}}^{450}} \times \frac{E_{\mathrm{sam}}}{E_{\mathrm{std}}} \qquad \text{Equation (S4)}$$

where Φ is the quantum yield, A^{450} is the absorbance at 450 nm (always kept below 0.1 for a 4 mm path length), E is the integrated emission peak of singlet oxygen at 1270 nm or the integrated phosphorescence emission peak between 520 and 950 nm, and *sam* and *std* denote the sample and standard, respectively.

5) Absolute phosphorescence quantum yield of $[Ru(bpy)_3]Cl_2$

The phosphorescence quantum yield (Φ_P) of $[Ru(bpy)_3]Cl_2$ in deuterated methanol in air at room temperature (293 ± 2 K) was determined by absolute methods using an integrating sphere-based setup, to serve as a standard for relative phosphorescence quantum yield measurements. Φ_P was found to be 0.015 ± 0.002. In order to validate the method used, Φ_P was also determined in water, where we obtained a Φ_P in air of 0.044 ± 0.005, which compares well to the literature value (0.040 ± 0.002).[5]

Experimental setup: The integrating sphere setup used for determining the phosphorescence quantum yield is depicted in Scheme S4. The excitation source was a fibre-coupled CW 450-nm diode laser (LRD-0450, Laserglow), coupled into a 200-µm multimode optical fibre, leading to a collimating lens (F220SMA-B, Thorlabs). After collimation, the light passed a mechanical iris to produce a 4-mm diameter beam (*vide infra*) with 10 mW optical power (P_{exc} = 80 mW·cm^{-2}). The excitation power was measured using a S310C thermal sensor connected to a PM100USB power meter (Thorlabs). A PTFE-coated AvaSphere-30-IRRAD integrating sphere (30 mm diameter, reflectance > 98%), fitted with three ports (entry, exit and sample port), and an AvaSpec-ULS2048L StarLine CCD spectrometer were obtained from Avantes. The integrating sphere and spectrometer were calibrated together using an Avalight-HAL-CAL-ISP30 NIST traceable calibration lamp from Avantes (9.5% relative uncertainty *versus* NIST standard), so that the observed intensities are expressed as a photon flux (mol photons·s^{-1}·nm^{-1}). The filter holder was fabricated by our own mechanical department, and held a NE520A (OD = 2) absorptive neutral density filter (Thorlabs) or a 500-nm longpass filter (FEL0500, Thorlabs, $T_{520\text{-}1000\,nm}$ = 92.1 ± 0.9%). An Avalight-DHc (Avantes) deuterium-halogen lamp was used as a white-light source for the determination of the transmission functions of the filters used. The spectra were recorded with Avasoft 8.5 software from Avantes, and further processed with Microsoft Office Excel 2010 and Origin Pro 9.1 software.

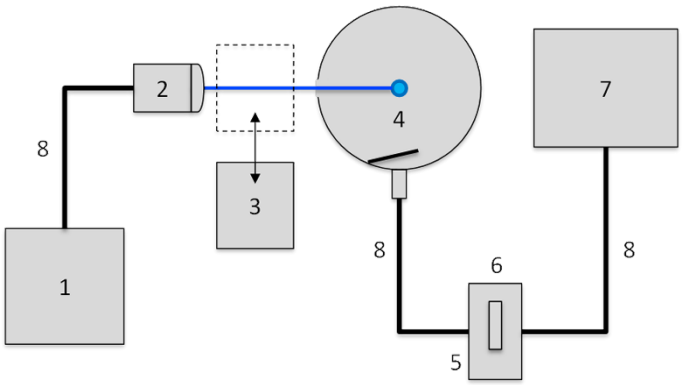

Scheme S4. Setup used for absolute quantum yield measurements. (1) laser source, (2) collimating lens, and mechanical iris, (3) power meter (adjustable in position), (4) integrating sphere with sample tube in the centre, (5) filter holder, (6) 500-nm longpass filter or OD2 neutral density filter, (7) CCD spectrometer, (8) optical fibres.

Experimental procedure: A measurement tube, made of a quartz EPR-tube bottom (± 7 cm length) fused to a NS-14 glass connector (± 2 cm length), was filled with a solution of $[Ru(bpy)_3]Cl_2$ (50 µL, 50 µM in CD_3OD), and closed with a septum under air. A second tube was filled with CD_3OD (50 µL) and served as the blank. The tube precisely fitted into a hole made in the integrating sphere, and was suspended in the centre of the sphere, in the middle of the excitation laser beam. The laser diode was allowed to warm up for 10 minutes prior to the experiment to guarantee a stable optical power output. The measurements were always performed in the same order, i.e. (1) absorption measurement of the blank, (2) absorption measurement of the sample, and (3) emission measurement of the sample. In this way, the neutral density filter is not moved between the measurement of the blank and sample, ensuring equal attenuation of the non-absorbed excitation light for both spectra. Equally, the sample

is not moved between the measurement of its absorption and emission. For the absorption measurements, the neutral density filter was placed in the filter, and replaced by the 500-nm longpass filter for the emission measurement.

Quantum yield calculation method: The phosphorescence quantum yield (Φ_P) is defined by Equation S5:

$$\Phi_P = \frac{q_{p\text{-em}}}{q_{p\text{-abs}}} = \frac{\int_{\lambda_1}^{\lambda_2} I_P(\lambda)d\lambda}{\int_{\lambda_3}^{\lambda_4}(I_{exc\text{-blank}}(\lambda) - I_{exc\text{-sample}}(\lambda))d\lambda} \quad \text{Equation (S5)}$$

Here, $q_{p\text{-em}}$ is the emission photon flux (in photons·s^{-1}) integrated over the spectral range λ_1 to λ_2 (520–950 nm), $q_{p\text{-abs}}$ is the photon flux absorbed by the ruthenium complex (in photons·s^{-1}), and $I_P(\lambda)$ is the spectral luminescence intensity (in photons·s^{-1}·nm^{-1}). $q_{p\text{-abs}}$ is determined by subtracting the spectral light intensity of the excitation source that has passed through the sample ($I_{exc\text{-sample}}$, in photons·s^{-1}·nm^{-1}) from the spectral light intensity of the excitation source that has passed through the blank sample ($I_{exc\text{-blank}}$, in photons·s^{-1}·nm^{-1}), and by integrating over the excitation wavelength range λ_3 to λ_4 (400–500 nm).

The spectrometer and the integrating sphere were calibrated so that the observed intensities are directly proportional to the photon flux, i.e. $I_P(\lambda) \propto$ [mol photons·s^{-1}·nm^{-1}] Therefore, integrating these values over the relevant wavelength regions directly provided the flux of photons that arrived at the spectrometer.

Because the intensity of the emitted light is relatively low compared to that of the exciting laser source the absorption and emission of the sample cannot be measured at the same time. In other words, the laser light saturates the spectrometer, which prevents the emission to be measured simultaneously. To circumvent this problem, the absorption was measured using a neutral density filter with known transmittance (typically $F_{attn} \approx 0.0062$, i.e. ~ 99.4% attenuation). This filter was placed between the integrating sphere and the spectrometer to measure the absorbed photon flux. The data was corrected for the attenuation by the neutral density filter ($F_{attn}(\lambda)$) at each wavelength. For the measurement of the emission, this filter was replaced by a longpass filter (> 500 nm) to remove the excitation light. Additionally, the intensity of the emission measured was corrected for the minimal absorbance of this light by the shortpass filter used. This was performed by dividing the luminescence intensity at each wavelength by the transmission curve $T(\lambda)$ of the longpass filter at this wavelength. The accordingly corrected equation for Φ_{UC} is Equation S6:

$$\Phi_P = \frac{\int_{\lambda_1}^{\lambda_2}\left(\frac{I_P(\lambda)}{T(\lambda)}\right)d\lambda}{\int_{\lambda_3}^{\lambda_4}\frac{I_{exc\text{-blank}}(\lambda) - I_{exc\text{-sample}}(\lambda)}{F_{attn}(\lambda)}d\lambda} \equiv \frac{q_{p\text{-em}}}{q_{p\text{-abs}}} \quad \text{Equation (S6)}$$

6) DFT-minimized structures: comparison

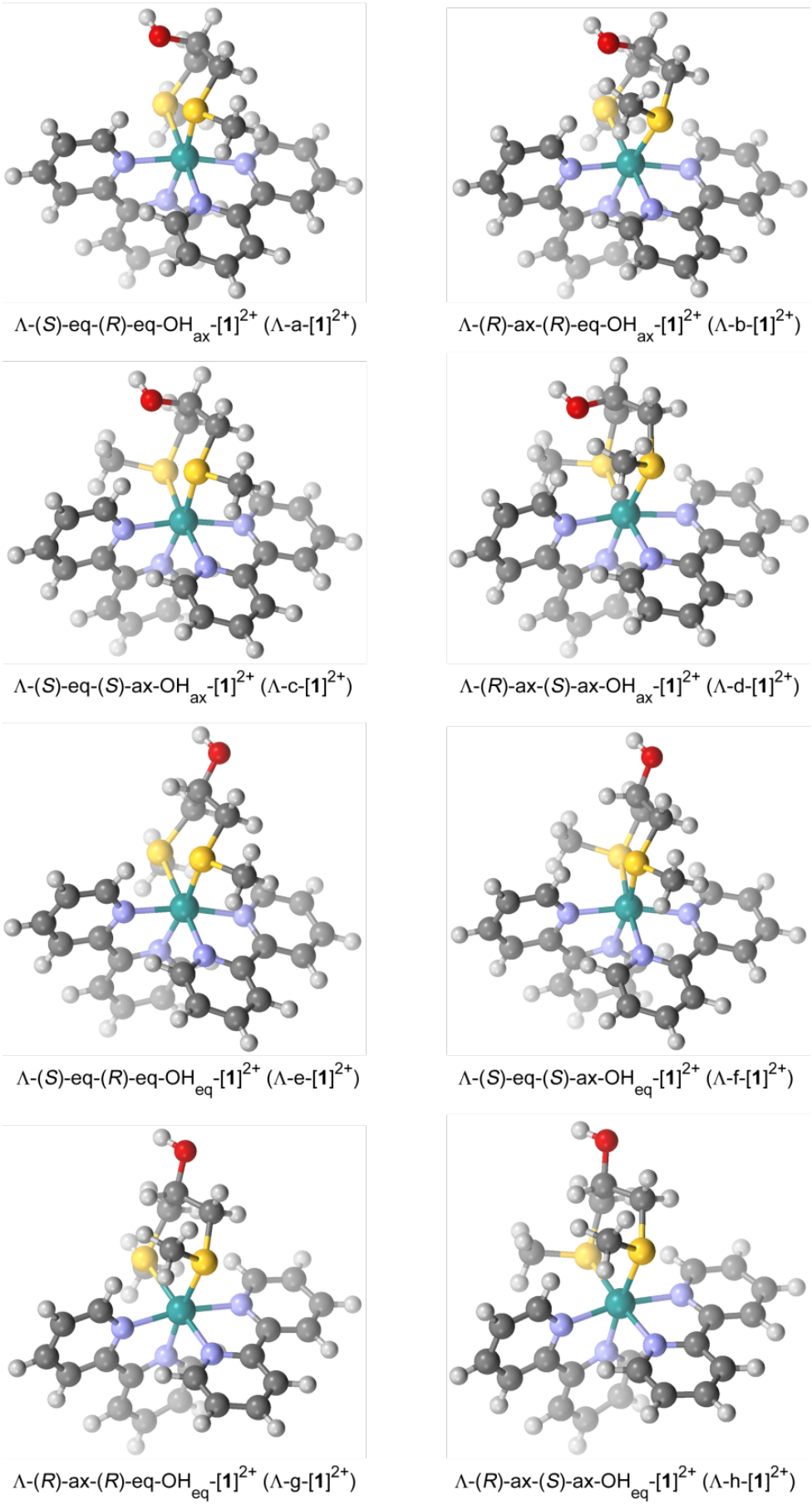

Figure S1. Structures of the isomers of $[1]^{2+}$ optimized by DFT in water (COSMO).

Table S2. Calculated bond lengths (Å), bond angles (°), and structural distortion parameters in DFT-minimized geometries of complex $[1]^{2+}$ in water.

	Λ-a-$[1]^{2+}$	Λ-b-$[1]^{2+}$	Λ-c-$[1]^{2+}$	Λ-d-$[1]^{2+}$	Λ-e-$[1]^{2+}$	Λ-f-$[1]^{2+}$	Λ-g-$[1]^{2+}$	Λ-h-$[1]^{2+}$
Ru-S1	2.441	2.476	2.428	2.471	2.442	2.427	2.475	2.471
Ru-S2	2.467	2.449	2.456	2.449	2.464	2.453	2.447	2.451
Ru-N11	2.145	2.143	2.148	2.141	2.149	2.150	2.146	2.148
Ru-N12	2.142	2.131	2.146	2.133	2.146	2.144	2.132	2.132
Ru-N21	2.136	2.140	2.140	2.139	2.138	2.140	2.139	2.139
Ru-N22	2.141	2.150	2.141	2.145	2.143	2.143	2.149	2.148
S1-Ru-S2	88.7	92.8	93.1	96.7	87.9	93.2	92.3	96.8
S1-Ru-N11	94.0	105.3	93.5	104.5	94.1	93.7	105.6	105.2
S1-Ru-N21	91.8	85.0	91.7	85.5	91.7	91.8	85.5	84.8
S1-Ru-N22	93.1	82.4	94.0	82.9	93.5	93.9	82.5	82.9
S2-Ru-N11	83.4	83.2	92.6	92.4	84.0	92.7	83.4	91.9
S2-Ru-N12	91.8	93.8	87.3	88.6	91.6	87.1	93.8	88.0
S2-Ru-N22	103.5	103.8	95.0	94.4	103.6	95.2	104.1	95.5
N11-Ru-N12	77.2	77.2	77.1	77.1	77.1	77.1	77.1	77.1
N11-Ru-N21	95.7	96.1	94.5	95.3	95.1	94.2	95.6	94.8
N12-Ru-N21	87.6	88.5	89.2	89.0	88.6	89.1	88.4	90.1
N12-Ru-N22	95.5	94.4	95.4	94.8	95.2	95.2	94.0	94.1
N21-Ru-N22	77.3	77.2	77.3	77.4	77.3	77.3	77.3	77.4
σ^2 [a]	59.4	87.5	41.6	66.5	58.4	41.7	87.2	68.9
Δ_{oct} [b]	0.0043	0.0046	0.0040	0.0045	0.0042	0.0039	0.0045	0.0045

[a] The bond angle variance is $\sigma^2 = \frac{1}{11}\sum_{n=1}^{12}(\theta_n - 90)^2$, where θ_n is one of the twelve angles in Table S2; [b] The mean-square relative deviation from average bond length is $\Delta_{\mathrm{oct}} = \frac{1}{6}\sum_{n=1}^{6}\left(\frac{d_n - \bar{d}}{\bar{d}}\right)^2$, where d_n is one of the six bond lengths in Table S2 and $\bar{d}$ is the average of those six bond lengths.

7) DFT-minimized structures: cartesian coordinates

Λ-(*S*)-eq-(*R*)-eq-OH_{ax}-$[1]^{2+}$ (Λ-a-$[1]^{2+}$)

Atom	X (Å)	Y (Å)	Z (Å)	Atom	X (Å)	Y (Å)	Z (Å)
1.C	-2.47835	2.72743	1.345942	**43.C**	-5.82143	0.019977	3.236314
2.S	-1.9813	1.403305	0.157304	**44.C**	-5.42023	0.486611	4.492407
3.C	-0.25032	2.022358	-0.16556	**45.C**	-4.05765	0.58963	4.771296
4.C	0.550809	1.180293	-1.16604	**46.H**	-3.40105	-0.05635	-1.5288
5.H	1.438988	1.783662	-1.41048	**47.H**	-5.11636	-0.69096	1.318945
6.C	1.105799	-0.15151	-0.6325	**48.H**	-0.94033	-2.62769	3.600972
7.S	-0.17595	-1.47152	-0.34303	**49.H**	1.056726	-0.34984	2.218326
8.C	0.939138	-2.75384	0.383123	**50.H**	-4.71295	-4.71552	-0.68162
9.H	-2.40745	3.684728	0.822389	**51.H**	-4.8858	-1.19326	-3.16138
10.H	-3.51699	2.535414	1.623563	**52.H**	-3.72952	0.95196	5.74019
11.H	-1.83471	2.722526	2.22897	**53.H**	-6.87118	-0.07643	2.971764
12.H	0.284479	2.087871	0.787262	**54.H**	-4.01873	-5.51765	1.085165
13.H	-0.38518	3.031681	-0.5669	**55.H**	-1.3816	-4.9236	4.445756
14.O	-0.25816	1.006661	-2.3592	**56.H**	-1.70062	1.050512	6.028536
15.H	0.771794	1.135632	6.251138	**57.H**	2.188237	0.412299	4.284042
16.H	1.78707	-0.58504	-1.37308	**58.H**	-5.56986	-3.58759	-2.72347
17.H	1.67249	0.02526	0.287877	**59.H**	-6.15498	0.765752	5.243733
18.H	1.375457	-2.42009	1.328336	**60.H**	-2.96833	-6.40657	3.153703
19.H	0.327602	-3.64517	0.54004	**61.H**	0.318188	0.630815	-3.05498
20.H	1.722791	-2.96661	-0.34926				
21.C	0.315778	0.796532	5.324224				
22.C	-1.07168	0.748316	5.197461				
23.C	-1.65481	0.307264	3.999126				
24.N	-0.87719	-0.08192	2.928975				
25.C	0.472093	-0.03067	3.072811				
26.C	1.102394	0.39722	4.239098				
27.Ru	-1.95718	-0.79278	1.222948				
28.N	-2.1817	-2.79798	1.941801				
29.C	-3.03928	-3.59435	1.224302				
30.C	-3.33268	-4.89839	1.653831				
31.C	-2.74451	-5.39736	2.81613				
32.C	-1.8663	-4.58008	3.53571				
33.C	-1.61449	-3.29125	3.06944				
34.C	-3.60202	-2.9897	-0.00083				
35.N	-3.24561	-1.68292	-0.24306				
36.C	-3.71074	-1.08453	-1.36865				
37.C	-4.54505	-1.72931	-2.27938				
38.C	-4.92025	-3.05388	-2.03389				
39.C	-4.44097	-3.68481	-0.88623				
40.C	-3.11501	0.225314	3.796418				
41.N	-3.51923	-0.23102	2.567126	**Energy**	−8190.30	kcal·mol^{-1}	
42.C	-4.84527	-0.32809	2.304751				

Λ-(*R*)-ax-(*R*)-eq-OH_{ax}-$[1]^{2+}$ (Λ-b-$[1]^{2+}$)

Atom	X (Å)	Y (Å)	Z (Å)	Atom	X (Å)	Y (Å)	Z (Å)
1.C	-2.914884	2.165797	-0.770203	**43.C**	-5.780352	0.12114	3.147472
2.S	-1.815431	1.531819	0.573837	**44.C**	-5.371154	0.674671	4.365103
3.C	-0.14877	2.049627	-0.071347	**45.C**	-4.008183	0.745697	4.651137
4.C	0.567131	1.196715	-1.128985	**46.H**	-3.273833	-0.202683	-1.633301
5.H	1.454707	1.7868	-1.409974	**47.H**	-5.086684	-0.759959	1.297871
6.C	1.119117	-0.152952	-0.639652	**48.H**	-0.853763	-2.68961	3.536716
7.S	-0.170217	-1.475515	-0.40916	**49.H**	1.092554	-0.584747	2.248942
8.C	0.941687	-2.808053	0.226761	**50.H**	-4.777796	-4.760679	-0.61291
9.H	-2.820068	3.255769	-0.767033	**51.H**	-4.799574	-1.333813	-3.227963
10.H	-2.63277	1.762455	-1.743301	**52.H**	-3.674419	1.171437	5.591748
11.H	-3.937411	1.888975	-0.499612	**53.H**	-6.83103	0.040873	2.880847
12.H	0.483889	2.124202	0.818666	**54.H**	-4.061991	-5.550018	1.152669
13.H	-0.301904	3.062763	-0.457164	**55.H**	-1.304542	-4.966837	4.417329
14.O	-0.299921	1.054393	-2.283809	**56.H**	-1.656177	1.106572	5.945928
15.H	0.811769	1.062507	6.219108	**57.H**	2.225201	0.187236	4.312557
16.H	1.79814	-0.564161	-1.395245	**58.H**	-5.596216	-3.673735	-2.69326
17.H	1.687212	-0.013908	0.286407	**59.H**	-6.100532	1.04516	5.08189
18.H	1.400278	-2.531568	1.179893	**60.H**	-2.964562	-6.433699	3.200038
19.H	0.32218	-3.699914	0.347766	**61.H**	0.222094	0.634379	-2.997086
20.H	1.70934	-2.991548	-0.530181				
21.C	0.356155	0.716453	5.294485				
22.C	-1.028872	0.742588	5.13866				
23.C	-1.612145	0.293624	3.943313				
24.N	-0.835246	-0.179096	2.909349				
25.C	0.511338	-0.201107	3.079463				
26.C	1.141638	0.232774	4.243104				
27.Ru	-1.924254	-0.864706	1.187489				
28.N	-2.14799	-2.854503	1.91668				
29.C	-3.040853	-3.645345	1.236508				
30.C	-3.34742	-4.937335	1.692907				
31.C	-2.732246	-5.433568	2.841941				
32.C	-1.813552	-4.625003	3.520029				
33.C	-1.553802	-3.346414	3.031881				
34.C	-3.607674	-3.053211	0.009354				
35.N	-3.211336	-1.764626	-0.270227				
36.C	-3.638055	-1.200608	-1.427563				
37.C	-4.491352	-1.845908	-2.320247				
38.C	-4.925983	-3.141173	-2.022897				
39.C	-4.471007	-3.747508	-0.852471				
40.C	-3.072256	0.270899	3.718441				
41.N	-3.483457	-0.259084	2.522549	**Energy**	−8187.29	kcal·mol^{-1}	
42.C	-4.809817	-0.331637	2.255757				

Λ-(*S*)-eq-(*S*)-ax-OH_{ax}-$[1]^{2+}$ (Λ-c-$[1]^{2+}$)

Atom	X (Å)	Y (Å)	Z (Å)	Atom	X (Å)	Y (Å)	Z (Å)
1.C	-2.512305	2.736959	1.345301	**43.C**	-5.837058	-0.004807	3.201194
2.S	-1.99883	1.416269	0.15967	**44.C**	-5.449044	0.485705	4.452395
3.C	-0.286874	2.067708	-0.17888	**45.C**	-4.089403	0.604073	4.738227
4.C	0.522271	1.229904	-1.175589	**46.H**	-3.457387	-0.005337	-1.50304
5.H	1.380156	1.860469	-1.458374	**47.H**	-5.115314	-0.7318	1.298473
6.C	1.151985	-0.054002	-0.602666	**48.H**	-0.764737	-2.673398	3.458572
7.S	0.07478	-1.454858	-0.011287	**49.H**	1.059281	-0.404778	2.276358
8.C	-0.312437	-2.278337	-1.621693	**50.H**	-4.80523	-4.648818	-0.628427
9.H	-2.46533	3.693258	0.816863	**51.H**	-5.062755	-1.092359	-3.051484
10.H	-3.544807	2.526427	1.632741	**52.H**	-3.770924	0.984507	5.703327
11.H	-1.861034	2.750409	2.222818	**53.H**	-6.883982	-0.115325	2.93086
12.H	0.251422	2.155472	0.770078	**54.H**	-3.924111	-5.533437	1.007148
13.H	-0.4447	3.069436	-0.591307	**55.H**	-1.105036	-5.01319	4.229739
14.O	-0.300162	0.991186	-2.347149	**56.H**	-1.750631	1.07538	6.019077
15.H	0.718606	1.143463	6.280102	**57.H**	2.159626	0.373958	4.348069
16.H	1.809721	-0.511979	-1.349692	**58.H**	-5.767555	-3.478977	-2.597342
17.H	1.776028	0.211916	0.257593	**59.H**	-6.191142	0.770191	5.194548
18.H	-0.878445	-3.180962	-1.379754	**60.H**	-2.739558	-6.477053	2.976186
19.H	-0.88615	-1.61581	-2.270681	**61.H**	0.297087	0.739254	-3.079435
20.H	0.639767	-2.55499	-2.082908				
21.C	0.274439	0.799793	5.34909				
22.C	-1.111104	0.764414	5.199466				
23.C	-1.679482	0.320012	3.994946				
24.N	-0.887527	-0.079493	2.939549				
25.C	0.460404	-0.05355	3.109629				
26.C	1.074692	0.377025	4.282815				
27.Ru	-1.94342	-0.771605	1.210727				
28.N	-2.105297	-2.805278	1.87579				
29.C	-2.981808	-3.59265	1.172762				
30.C	-3.222796	-4.919626	1.563097				
31.C	-2.557033	-5.450087	2.668474				
32.C	-1.652135	-4.643606	3.366459				
33.C	-1.455739	-3.330961	2.941341				
34.C	-3.612895	-2.956722	-0.002963				
35.N	-3.246029	-1.652965	-0.252082				
36.C	-3.773856	-1.030432	-1.336967				
37.C	-4.676099	-1.647386	-2.20063				
38.C	-5.061164	-2.967977	-1.947518				
39.C	-4.521941	-3.622821	-0.840722				
40.C	-3.136455	0.233919	3.775429				
41.N	-3.527469	-0.241334	2.548283	**Energy**	−8190.42	kcal·mol^{-1}	
42.C	-4.851503	-0.35591	2.281023				

Λ-(*R*)-ax-(*S*)-ax-OH_{ax}-$[1]^{2+}$ (Λ-d-$[1]^{2+}$)

Atom	X (Å)	Y (Å)	Z (Å)	Atom	X (Å)	Y (Å)	Z (Å)
1.C	-3.132175	2.213236	-0.541399	**43.C**	-5.826253	0.048937	3.082408
2.S	-1.8061	1.577603	0.582203	**44.C**	-5.457458	0.587393	4.319655
3.C	-0.290331	2.06706	-0.376871	**45.C**	-4.102577	0.699867	4.629644
4.C	0.302072	1.087448	-1.40003	**46.H**	-3.162268	-0.151947	-1.668242
5.H	1.066339	1.672925	-1.936675	**47.H**	-5.07426	-0.766754	1.227819
6.C	1.073165	-0.101424	-0.791341	**48.H**	-0.762884	-2.698671	3.469062
7.S	0.145331	-1.489117	0.033343	**49.H**	1.079274	-0.516939	2.338017
8.C	-0.200208	-2.562575	-1.432365	**50.H**	-4.847193	-4.634393	-0.594077
9.H	-3.086464	3.305165	-0.497755	**51.H**	-4.783186	-1.217505	-3.220512
10.H	-2.990383	1.868124	-1.566036	**52.H**	-3.799046	1.11438	5.58545
11.H	-4.087137	1.869296	-0.135968	**53.H**	-6.868766	-0.060843	2.795072
12.H	0.465067	2.298359	0.38068	**54.H**	-4.03401	-5.497647	1.094487
13.H	-0.565548	3.002959	-0.872757	**55.H**	-1.194883	-4.999783	4.30296
14.O	-0.731429	0.68493	-2.333065	**56.H**	-1.783542	1.175541	5.95286
15.H	0.678799	1.192346	6.274287	**57.H**	2.149779	0.321225	4.410528
16.H	1.669406	-0.595781	-1.565669	**58.H**	-5.669659	-3.517658	-2.656317
17.H	1.770608	0.27137	-0.032248	**59.H**	-6.211437	0.91354	5.032391
18.H	-0.684499	-3.465976	-1.053754	**60.H**	-2.891958	-6.430452	3.094791
19.H	-0.840171	-2.047766	-2.15008	**61.H**	-0.288488	0.370279	-3.146097
20.H	0.762888	-2.824064	-1.879282				
21.C	0.249504	0.823256	5.345861				
22.C	-1.132322	0.815776	5.162818				
23.C	-1.680873	0.338944	3.961362				
24.N	-0.871564	-0.126416	2.950559				
25.C	0.472186	-0.121119	3.146819				
26.C	1.067039	0.342578	4.317408				
27.Ru	-1.899683	-0.813077	1.197847				
28.N	-2.106173	-2.820789	1.886968				
29.C	-3.013159	-3.593945	1.205683				
30.C	-3.309777	-4.896943	1.635225				
31.C	-2.667041	-5.421703	2.756726				
32.C	-1.728137	-4.633192	3.429843				
33.C	-1.478308	-3.342291	2.968447				
34.C	-3.592653	-2.975639	-0.003697				
35.N	-3.151605	-1.702932	-0.294265				
36.C	-3.578391	-1.125709	-1.445793				
37.C	-4.476828	-1.738351	-2.317113				
38.C	-4.960353	-3.01307	-2.004742				
39.C	-4.502983	-3.636017	-0.844114				
40.C	-3.134283	0.276932	3.704875				
41.N	-3.506367	-0.243468	2.489904	**Energy**	−8186.91	kcal·mol^{-1}	
42.C	-4.826031	-0.350954	2.198752				

Λ-(*S*)-eq-(*R*)-eq-OH_{eq}-$[1]^{2+}$ (Λ-e-$[1]^{2+}$)

Atom	X (Å)	Y (Å)	Z (Å)	Atom	X (Å)	Y (Å)	Z (Å)
1.C	-2.449494	2.715713	1.423507	**43.C**	-5.84304	-0.005113	3.246207
2.S	-1.93605	1.406874	0.225413	**44.C**	-5.4482	0.410719	4.522053
3.C	-0.196391	2.002068	-0.054506	**45.C**	-4.08701	0.491783	4.814943
4.C	0.553066	1.159798	-1.098694	**46.H**	-3.381185	0.004712	-1.507398
5.O	1.671563	1.997367	-1.518085	**47.H**	-5.128512	-0.65446	1.310735
6.C	1.121134	-0.166609	-0.563826	**48.H**	-1.00117	-2.706138	3.593839
7.S	-0.178089	-1.480387	-0.30706	**49.H**	1.041012	-0.428232	2.284517
8.C	0.909702	-2.792128	0.408334	**50.H**	-4.782389	-4.643253	-0.74885
9.H	-2.357389	3.680807	0.918291	**51.H**	-4.871087	-1.077963	-3.169748
10.H	-3.495583	2.524915	1.671921	**52.H**	-3.763529	0.813908	5.799424
11.H	-1.825237	2.687078	2.319536	**53.H**	-6.891288	-0.081435	2.969417
12.H	0.337402	2.027976	0.901645	**54.H**	-4.12625	-5.485213	1.011387
13.H	-0.305101	3.022715	-0.435304	**55.H**	-1.505178	-5.001353	4.401985
14.H	-0.100518	0.971148	-1.962669	**56.H**	-1.738979	0.918344	6.097029
15.H	2.102285	1.554344	-2.277835	**57.H**	2.16	0.269835	4.379636
16.H	1.799934	-0.599015	-1.306971	**58.H**	-5.600901	-3.467112	-2.778044
17.H	1.676654	-0.000716	0.36536	**59.H**	-6.186544	0.668525	5.277354
18.H	1.346722	-2.471755	1.357278	**60.H**	-3.116922	-6.427327	3.076357
19.H	0.27904	-3.671242	0.555502	**61.H**	0.73166	0.970074	6.346486
20.H	1.690723	-3.013066	-0.324114				
21.C	0.281502	0.657158	5.407625				
22.C	-1.105027	0.627889	5.265652				
23.C	-1.68075	0.219989	4.051971				
24.N	-0.896627	-0.15086	2.980424				
25.C	0.451324	-0.120695	3.13977				
26.C	1.074682	0.270904	4.322486				
27.Ru	-1.968336	-0.806576	1.245245				
28.N	-2.233914	-2.821959	1.923236				
29.C	-3.103734	-3.587101	1.187381				
30.C	-3.430775	-4.890411	1.594507				
31.C	-2.865385	-5.419314	2.754802				
32.C	-1.973497	-4.633885	3.492674				
33.C	-1.686239	-3.345385	3.046861				
34.C	-3.643795	-2.95083	-0.031498				
35.N	-3.26116	-1.646766	-0.248669				
36.C	-3.708782	-1.020548	-1.366315				
37.C	-4.547478	-1.634786	-2.294245				
38.C	-4.948109	-2.956275	-2.074309				
39.C	-4.489235	-3.614913	-0.934243				
40.C	-3.139841	0.155892	3.834625				
41.N	-3.537638	-0.254748	2.58732	**Energy**	−8190.11	kcal·mol^{-1}	
42.C	-4.862097	-0.329346	2.310913				

Λ-(*S*)-eq-(*S*)-ax-OH_{eq}-$[1]^{2+}$ (Λ-f-$[1]^{2+}$)

Atom	X (Å)	Y (Å)	Z (Å)	Atom	X (Å)	Y (Å)	Z (Å)
1.C	-2.466862	2.730299	1.396157	**43.C**	-5.859283	0.013001	3.194976
2.S	-1.959007	1.405534	0.212114	**44.C**	-5.478497	0.484712	4.455366
3.C	-0.237127	2.018935	-0.124843	**45.C**	-4.120539	0.582017	4.756837
4.C	0.511841	1.1368	-1.134084	**46.H**	-3.460907	0.025065	-1.468094
5.O	1.573196	1.989632	-1.664751	**47.H**	-5.12694	-0.707162	1.294175
6.C	1.168981	-0.11084	-0.514595	**48.H**	-0.826805	-2.725546	3.485229
7.S	0.058951	-1.505067	0.035246	**49.H**	1.043155	-0.481073	2.350754
8.C	-0.331068	-2.241037	-1.616166	**50.H**	-4.854103	-4.61491	-0.652548
9.H	-2.396375	3.688206	0.873571	**51.H**	-5.067882	-1.028615	-3.034589
10.H	-3.506525	2.533305	1.666907	**52.H**	-3.807457	0.948183	5.729136
11.H	-1.827686	2.724378	2.282367	**53.H**	-6.904501	-0.081779	2.912418
12.H	0.309585	2.107038	0.820473	**54.H**	-3.99253	-5.526379	0.975407
13.H	-0.373226	3.015073	-0.558281	**55.H**	-1.196022	-5.069457	4.226643
14.H	-0.161725	0.853243	-1.954455	**56.H**	-1.792731	1.003441	6.070957
15.H	1.954579	1.536206	-2.444198	**57.H**	2.127596	0.261468	4.442724
16.H	1.850055	-0.576363	-1.235593	**58.H**	-5.793845	-3.415156	-2.613644
17.H	1.754839	0.171423	0.3661	**59.H**	-6.224714	0.770832	5.192675
18.H	-0.960114	-3.114096	-1.429203	**60.H**	-2.835627	-6.502777	2.94488
19.H	-0.851151	-1.527863	-2.25936	**61.H**	0.67324	1.033062	6.363995
20.H	0.614507	-2.556546	-2.065003				
21.C	0.236278	0.705968	5.423692				
22.C	-1.147468	0.692165	5.256022				
23.C	-1.706813	0.268706	4.039751				
24.N	-0.907531	-0.132422	2.990831				
25.C	0.438176	-0.128289	3.178647				
26.C	1.043862	0.282207	4.363573				
27.Ru	-1.953977	-0.79205	1.241474				
28.N	-2.154477	-2.82636	1.889093				
29.C	-3.031706	-3.597539	1.169734				
30.C	-3.289611	-4.925839	1.54355				
31.C	-2.639882	-5.47456	2.649596				
32.C	-1.732636	-4.685187	3.363277				
33.C	-1.519419	-3.370163	2.954203				
34.C	-3.64615	-2.942891	-0.004028				
35.N	-3.262479	-1.640981	-0.238053				
36.C	-3.783615	-1.000162	-1.315773				
37.C	-4.688623	-1.598067	-2.190018				
38.C	-5.086295	-2.917932	-1.954559				
39.C	-4.55819	-3.590278	-0.853054				
40.C	-3.162146	0.207398	3.801467				
41.N	-3.545955	-0.25009	2.565499	**Energy**	−8191.21	kcal·mol^{-1}	
42.C	-4.868335	-0.342439	2.28228				

Λ-(*R*)-ax-(*R*)-eq-OH_{eq}-$[1]^{2+}$ (Λ-g-$[1]^{2+}$)

Atom	X (Å)	Y (Å)	Z (Å)	Atom	X (Å)	Y (Å)	Z (Å)
1.C	-2.752547	2.133835	-0.87867	**43.C**	-5.824557	0.092065	3.138208
2.S	-1.81649	1.516585	0.58987	**44.C**	-5.427278	0.637634	4.363
3.C	-0.100312	2.003512	0.087793	**45.C**	-4.066623	0.712868	4.659787
4.C	0.566058	1.181117	-1.028926	**46.H**	-3.328802	-0.212369	-1.607086
5.O	1.684528	2.006214	-1.477875	**47.H**	-5.113707	-0.772135	1.287718
6.C	1.124374	-0.177393	-0.569941	**48.H**	-0.894571	-2.691257	3.572522
7.S	-0.188442	-1.485605	-0.378764	**49.H**	1.056655	-0.615407	2.305497
8.C	0.891704	-2.858047	0.227378	**50.H**	-4.776836	-4.789538	-0.598497
9.H	-2.621629	3.219369	-0.904764	**51.H**	-4.84176	-1.353924	-3.200609
10.H	-2.399996	1.68637	-1.811045	**52.H**	-3.741907	1.132186	5.60642
11.H	-3.805812	1.897705	-0.707358	**53.H**	-6.872743	0.009429	2.862802
12.H	0.492868	1.969927	1.007279	**54.H**	-4.068205	-5.571483	1.167438
13.H	-0.181168	3.049087	-0.227572	**55.H**	-1.344469	-4.966928	4.455646
14.H	-0.130906	1.038056	-1.866231	**56.H**	-1.727286	1.077547	5.974884
15.H	2.05837	1.584676	-2.27887	**57.H**	2.169091	0.149054	4.384002
16.H	1.788015	-0.576752	-1.345037	**58.H**	-5.607807	-3.706309	-2.675667
17.H	1.693498	-0.071557	0.359701	**59.H**	-6.164011	0.997802	5.077551
18.H	1.34935	-2.610827	1.189024	**60.H**	-2.985701	-6.444922	3.226866
19.H	0.251341	-3.738076	0.324838	**61.H**	0.737103	1.028738	6.274093
20.H	1.658638	-3.03904	-0.530498				
21.C	0.290829	0.684595	5.344267				
22.C	-1.092318	0.714734	5.173209				
23.C	-1.663846	0.271114	3.970251				
24.N	-0.876127	-0.197555	2.942743				
25.C	0.468066	-0.22972	3.129883				
26.C	1.086673	0.199001	4.301724				
27.Ru	-1.948879	-0.876376	1.20856				
28.N	-2.174179	-2.865154	1.941827				
29.C	-3.057224	-3.661646	1.255971				
30.C	-3.361213	-4.954198	1.712125				
31.C	-2.754533	-5.444761	2.868186				
32.C	-1.846275	-4.630124	3.552392				
33.C	-1.587326	-3.351754	3.062986				
34.C	-3.620922	-3.073434	0.025558				
35.N	-3.233974	-1.781467	-0.252595				
36.C	-3.673149	-1.217748	-1.405176				
37.C	-4.522855	-1.86796	-2.297836				
38.C	-4.941091	-3.169269	-2.005438				
39.C	-4.478591	-3.773635	-0.836978				
40.C	-3.121761	0.248381	3.731131				
41.N	-3.521621	-0.275836	2.528687	**Energy**	−8187.98	kcal·mol^{-1}	
42.C	-4.845224	-0.349263	2.250201				

Λ-(*R*)-ax-(*S*)-ax-OH_{eq}-$[1]^{2+}$ (Λ-h-$[1]^{2+}$)

Atom	X (Å)	Y (Å)	Z (Å)	Atom	X (Å)	Y (Å)	Z (Å)
1.C	-2.845053	2.175598	-0.791656	**43.C**	-5.845011	0.140712	3.114293
2.S	-1.841533	1.535651	0.622163	**44.C**	-5.450858	0.721582	4.32405
3.C	-0.153038	2.009637	0.030407	**45.C**	-4.09167	0.794431	4.625537
4.C	0.469249	1.130333	-1.067925	**46.H**	-3.412667	-0.136976	-1.556224
5.O	1.506691	1.965899	-1.669244	**47.H**	-5.133403	-0.781078	1.294303
6.C	1.136967	-0.152521	-0.538143	**48.H**	-0.80687	-2.740128	3.479998
7.S	0.036852	-1.564334	-0.016655	**49.H**	1.033269	-0.720272	2.385373
8.C	-0.363252	-2.25695	-1.684173	**50.H**	-4.874401	-4.714653	-0.573387
9.H	-2.718559	3.261943	-0.801744	**51.H**	-5.015078	-1.223081	-3.096779
10.H	-2.531932	1.750201	-1.748483	**52.H**	-3.768241	1.238471	5.56125
11.H	-3.889738	1.932621	-0.581801	**53.H**	-6.892128	0.056862	2.835136
12.H	0.478519	2.031295	0.924603	**54.H**	-4.019307	-5.58179	1.07987
13.H	-0.255921	3.035606	-0.337808	**55.H**	-1.179761	-5.059327	4.282947
14.H	-0.279605	0.886883	-1.833084	**56.H**	-1.760833	1.181478	5.94656
15.H	1.835355	1.502268	-2.466834	**57.H**	2.130348	0.085702	4.451444
16.H	1.78014	-0.587687	-1.311119	**58.H**	-5.787334	-3.577924	-2.585052
17.H	1.764917	0.077595	0.329134	**59.H**	-6.188166	1.11172	5.021876
18.H	-0.991446	-3.134865	-1.517585	**60.H**	-2.846227	-6.51511	3.0615
19.H	-0.886502	-1.52777	-2.306692	**61.H**	0.696726	1.076597	6.285359
20.H	0.57964	-2.560658	-2.146636				
21.C	0.254889	0.715883	5.359652				
22.C	-1.124013	0.777106	5.166586				
23.C	-1.689851	0.309971	3.969457				
24.N	-0.899026	-0.203029	2.966534				
25.C	0.441153	-0.275552	3.178807				
26.C	1.052001	0.17033	4.347768				
27.Ru	-1.959684	-0.86002	1.217489				
28.N	-2.15508	-2.869598	1.902239				
29.C	-3.045812	-3.655126	1.21502				
30.C	-3.307878	-4.971284	1.626404				
31.C	-2.647715	-5.496431	2.737045				
32.C	-1.726114	-4.694232	3.417284				
33.C	-1.509676	-3.391599	2.972821				
34.C	-3.658607	-3.031122	0.026238				
35.N	-3.2624	-1.739595	-0.246114				
36.C	-3.757492	-1.143278	-1.359861				
37.C	-4.658639	-1.762069	-2.223171				
38.C	-5.079877	-3.06457	-1.938473				
39.C	-4.569529	-3.699706	-0.80717				
40.C	-3.144692	0.296273	3.71687				
41.N	-3.540854	-0.258461	2.525618	**Energy**	−8188.05	kcal·mol^{-1}	
42.C	-4.864684	-0.333541	2.245262				

8) 2D NMR of $[1]^{2+}$

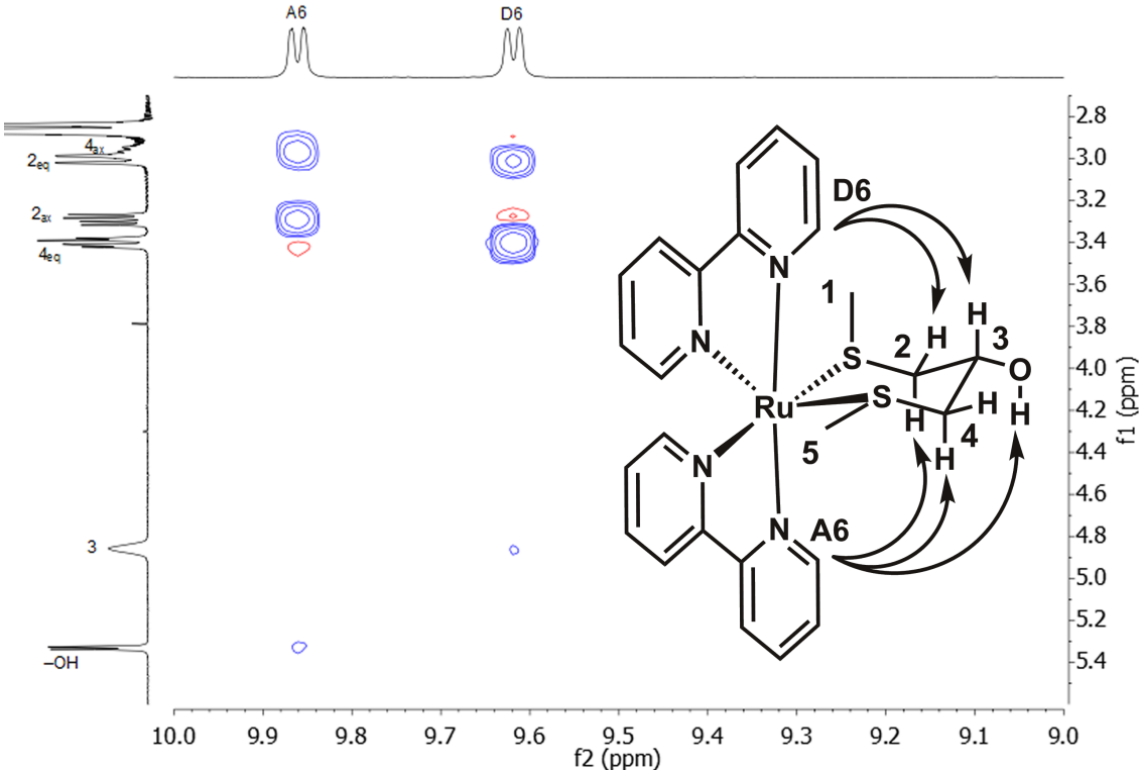

Figure S2. Partial ^{1}H NOESY NMR spectrum of a solution of $[1](PF_6)_2$ in acetone-*d6*, showing the off-diagonal peaks between the H_{A6} proton and $H_{2,ax}$, $H_{4,ax}$, and –OH protons, and the H_{D6} proton and $H_{2,eq}$, $H_{4,eq}$, H_3 protons. This confirms that the proton H3 is axial, and the –OH is thus oriented equatorially.

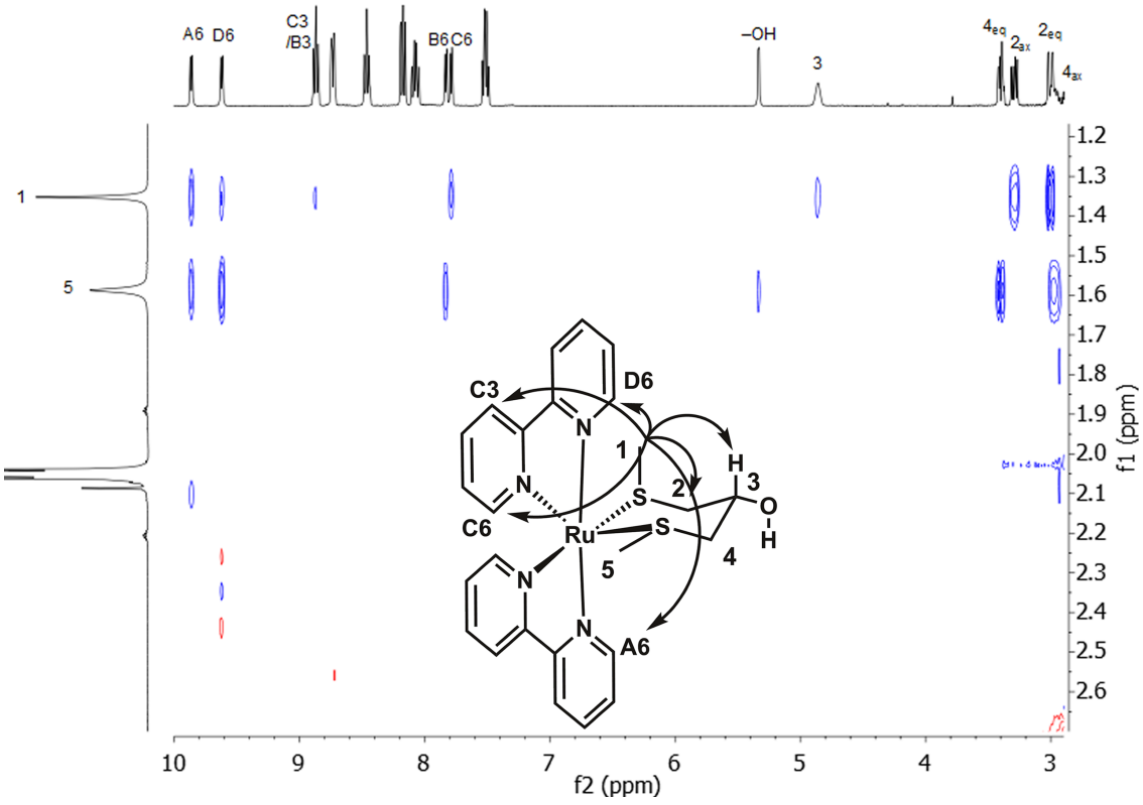

Figure S3. Partial ^{1}H NOESY NMR spectrum of a solution of $[1](PF_6)_2$ in acetone-*d6*, showing the off-diagonal peaks between the H_1 protons and the H_2, H_3, H_{A6}, H_{C3}, H_{C6}, and H_{D6} protons.

9) Dark stability and photochemistry of $[1]^{2+}$-$[3]^{2+}$

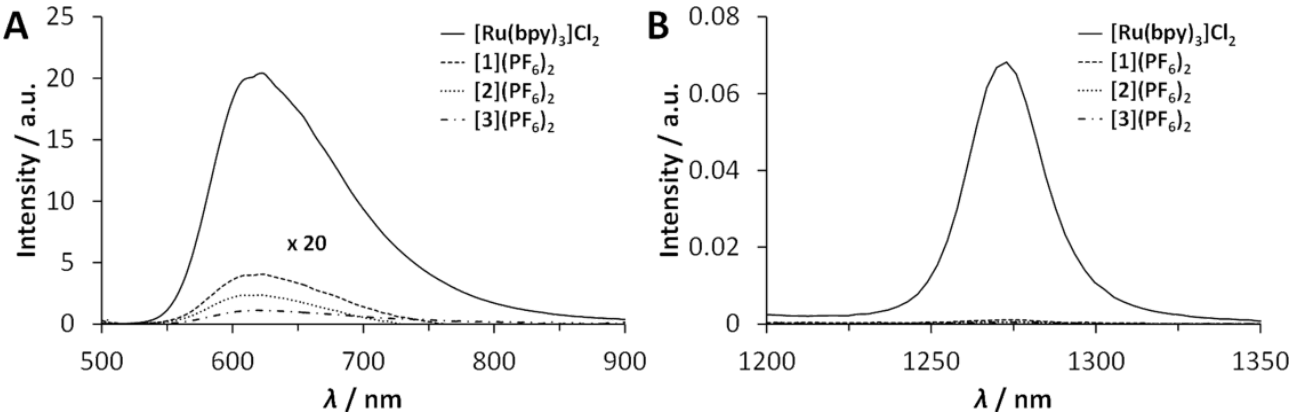

Figure S4. (a) Visible emission spectra of $[1](PF_6)_2$, $[2](PF_6)_2$, $[3](PF_6)_2$, and $[Ru(bpy)_3]Cl_2$ in aerated CD_3OD at 293 K under blue-light irradiation (450 nm, 0.4 W·cm^{-2}). (b) Near-infrared spectra of $^1O_2$ phosphorescence (λ_{em} = 1275 nm) sensitized by $[1](PF_6)_2$, $[2](PF_6)_2$, $[3](PF_6)_2$, and $[Ru(bpy)_3]Cl_2$ in aerated CD_3OD at 293 K under blue-light irradiation (450 nm, 0.4 W·cm^{-2}).

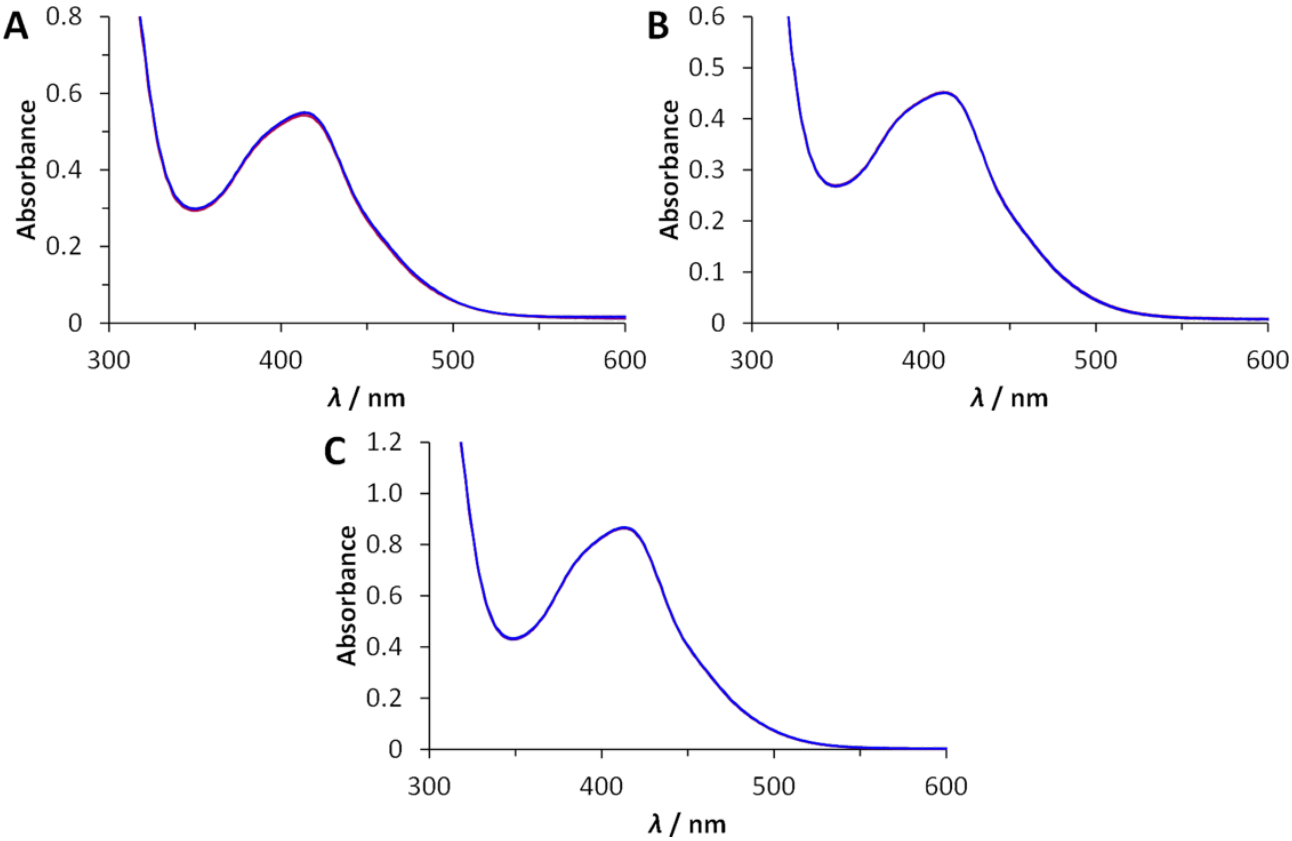

Figure S5. Evolution of the UV-Vis absorption spectra of solutions of (A) $[1](PF_6)_2$ (106 µM), (B) $[2](PF_6)_2$ (112 µM), and (C) $[3](PF_6)_2$ (167 µM) in H_2O in the dark for 53 h at 298 K under air.

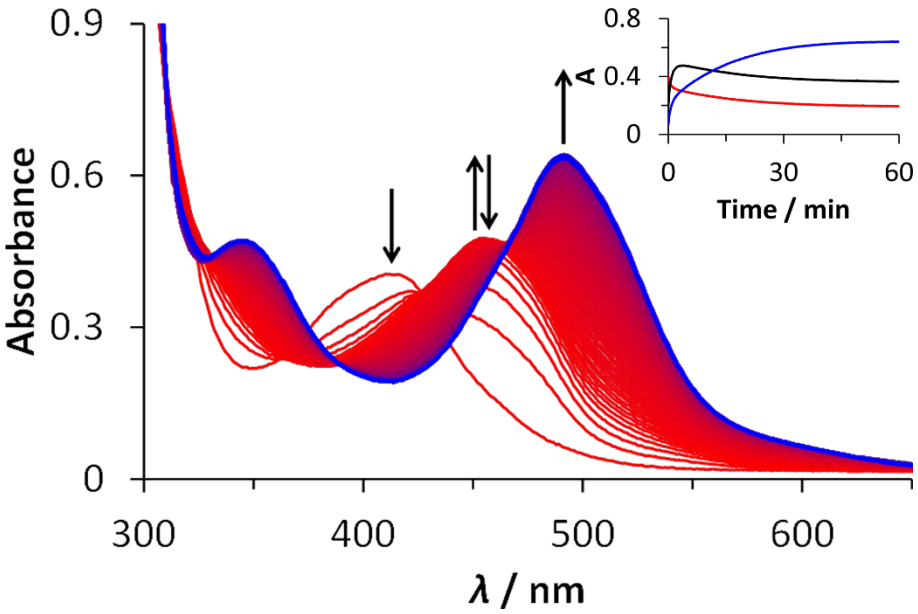

Figure S6. Evolution of the UV-Vis absorption spectra of a solution of $[1](PF_6)_2$ in H_2O (72 μM) upon irradiation (120 min) at 298 K with a 443 nm LED (q_p = 2.65 × 10^{-8} mol photons·s^{-1}) under N_2. Inset: Time evolution of the absorbance at 413 nm (red), 453 nm (black) and 491 nm (blue) during the irradiation.

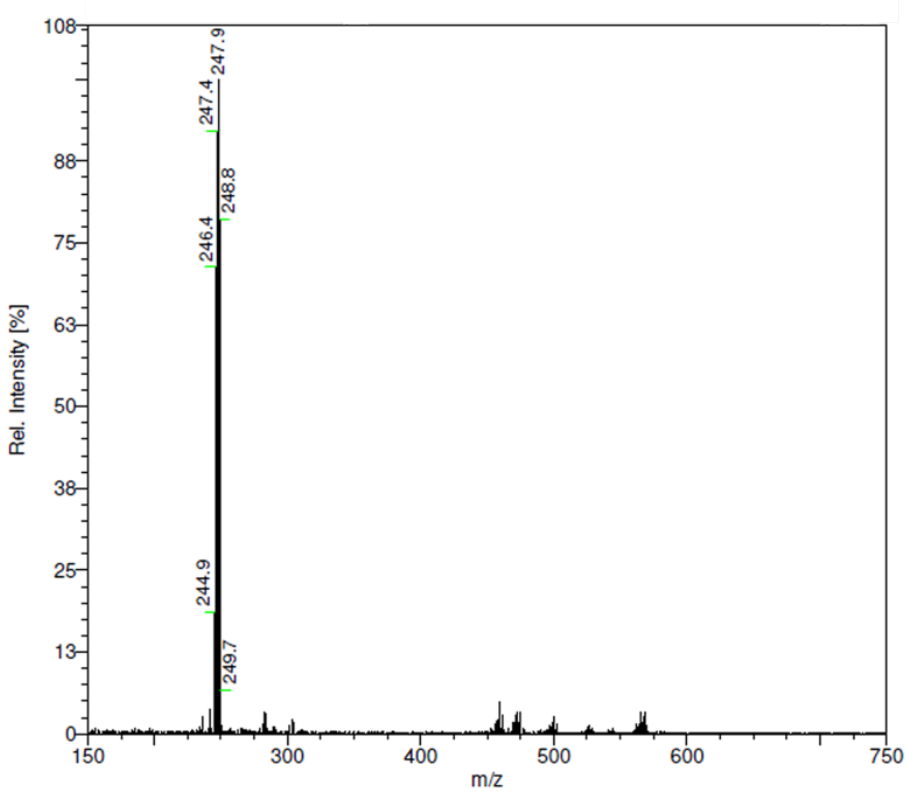

Figure S7. Mass spectrum taken in acetonitrile after 120 min of photolysis of an aqueous solution of $[1](PF_6)_2$ under N_2 at 298 K showing a peak corresponding to $[Ru(bpy)_2(CH_3CN)_2]^{2+}$ (calcd. m/z = 248.0).

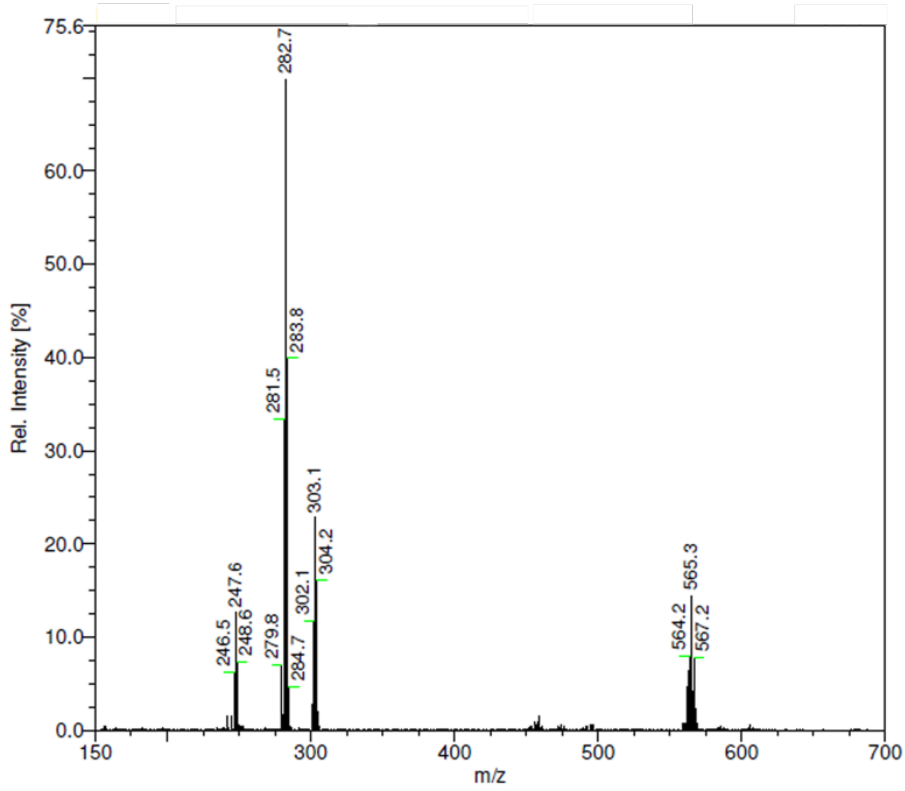

Figure S8. Mass spectrum taken in acetonitrile after 5 min of photolysis of an aqueous solution of $[1](PF_6)_2$ under N_2 at 298 K showing peaks corresponding to $[Ru(bpy)_2(CH_3CN)_2]^{2+}$ (calcd. m/z = 248.0), $[Ru(bpy)_2(4)]^{2+}$ (calcd. m/z = 283.0), $[Ru(bpy)_2(4)(CH_3CN)]^{2+}$ (calcd. m/z = 303.6), and $\{[Ru(bpy)_2(4)]-H\}^{+}$ (calcd. m/z = 565.1).

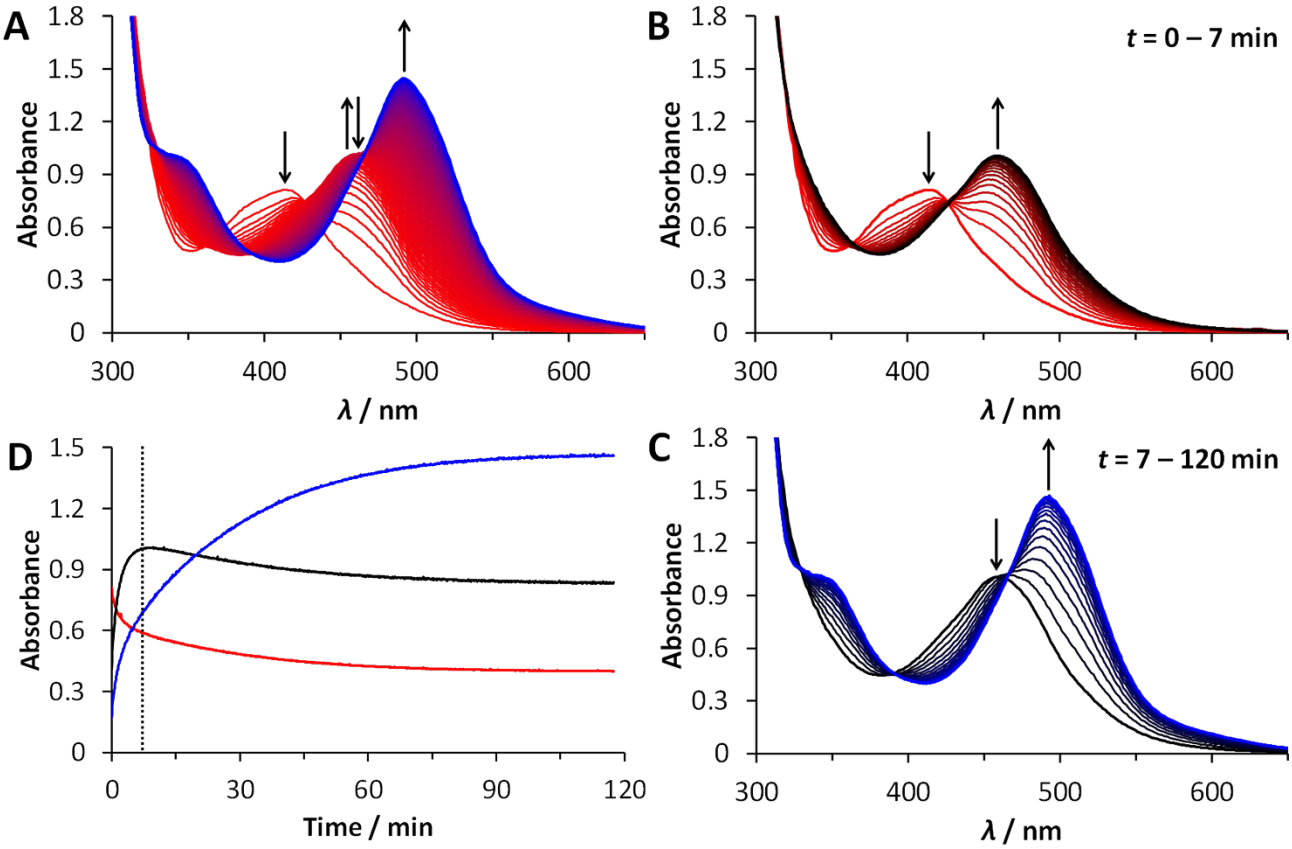

Figure S9. Evolution of the UV-Vis absorption spectra of a solution of [2](PF$_6$)$_2$ in H$_2$O (181 µM) upon irradiation (120 min) at 298 K with a 443 nm LED (q_p = 2.85 × 10^{-8} mol photons·s^{-1}) under N$_2$, showing both the overall reaction (A), as well as the spectral changes in the first 7 minutes (B, Δt = 24 s) and thereafter (C, Δt = 6.4 min) separately. Time evolution (D) of the absorbance at 412 nm (red), 456 nm (black) and 491 nm (blue) during the irradiation, whereby the vertical dashed line indicates the end of the first reaction (t = 7 min).

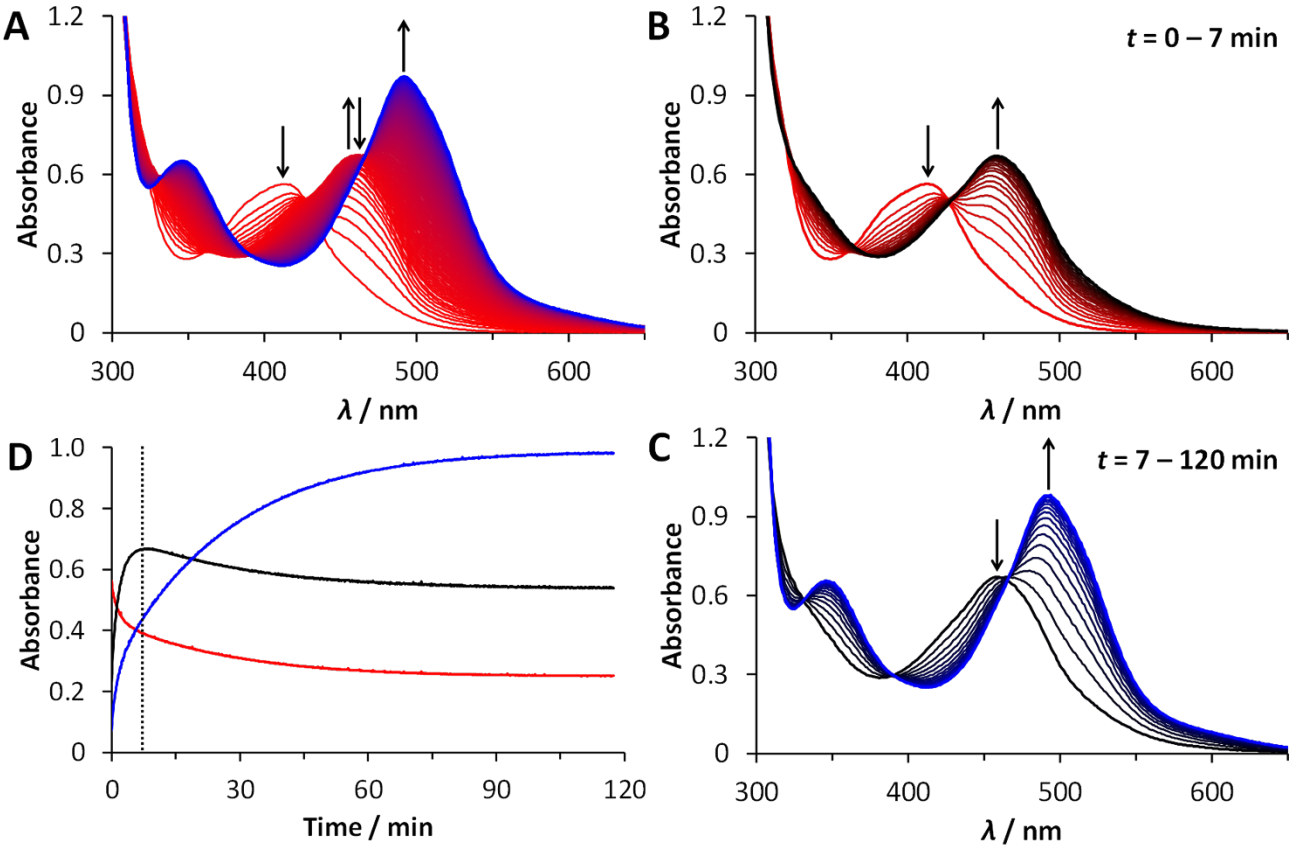

Figure S10. Evolution of the UV-Vis absorption spectra of a solution of [3](PF$_6$)$_2$ in H2O (99 µm) upon irradiation (120 min) at 298 K with a 443 nm LED (q_p = 2.85 × 10−8 mol photons·s−1) under N_2, showing both the overall reaction (A), as well as the spectral changes in the first 7 minutes (B, Δt = 24 s) and thereafter (C, Δt = 6.4 min) separately. Time evolution (D) of the absorbance at 412 nm (red), 456 nm (black) and 491 nm (blue) during the irradiation, whereby the vertical dashed line indicates the end of the first reaction (t = 7 min).

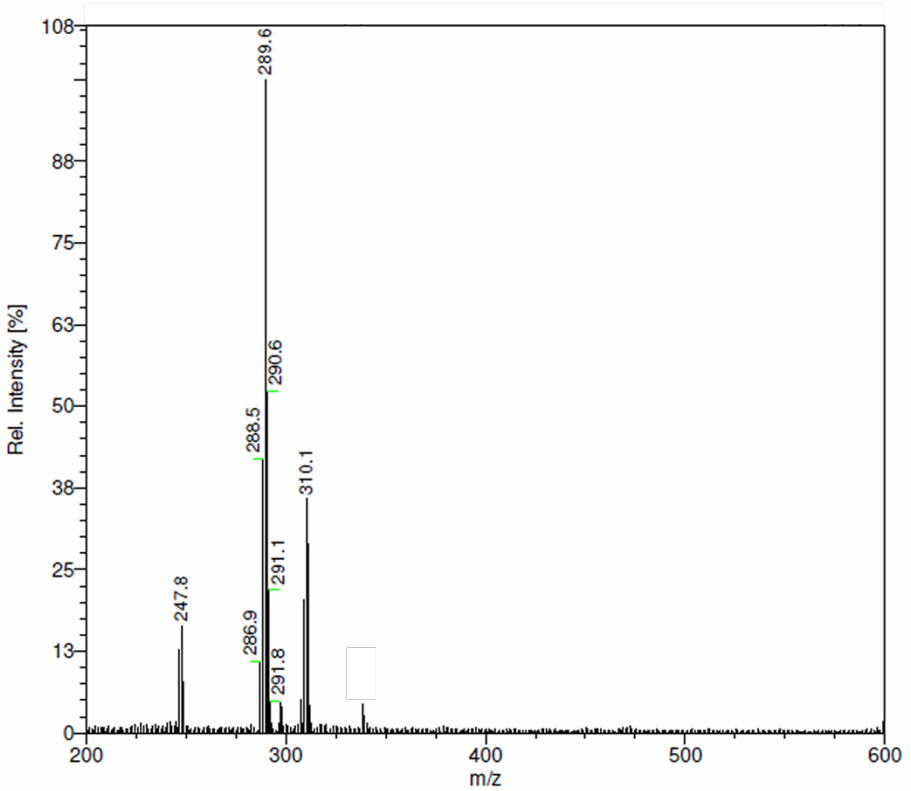

Figure S11. Mass spectrum taken in acetonitrile after 5 min of photolysis of an aqueous solution of $[2](PF_6)_2$ under N_2 at 298 K showing peaks corresponding to $[Ru(bpy)_2(CH_3CN)_2]^{2+}$ (calcd. m/z = 248.0), $[Ru(bpy)_2(5)]^{2+}$ (calcd. m/z = 290.0), and $[Ru(bpy)_2(5)(CH_3CN)]^{2+}$ (calcd. m/z = 310.6).

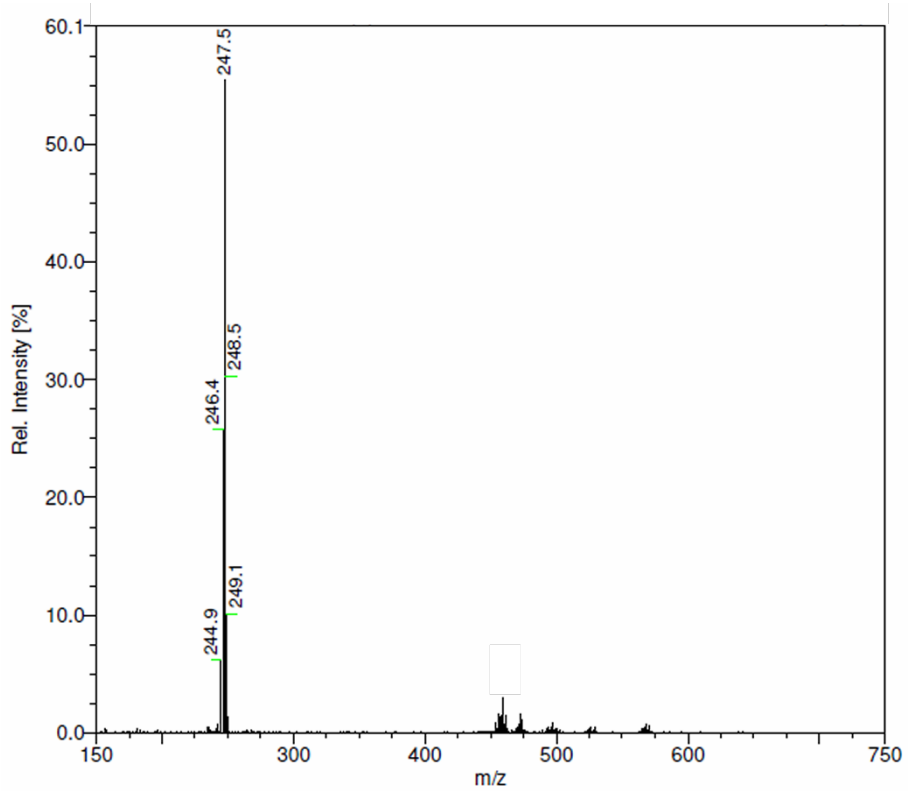

Figure S12. Mass spectrum taken in acetonitrile after 120 min of photolysis of an aqueous solution of $[2](PF_6)_2$ under N_2 at 298 K showing a peak corresponding to $[Ru(bpy)_2(CH_3CN)_2]^{2+}$ (calcd. m/z = 248.0).

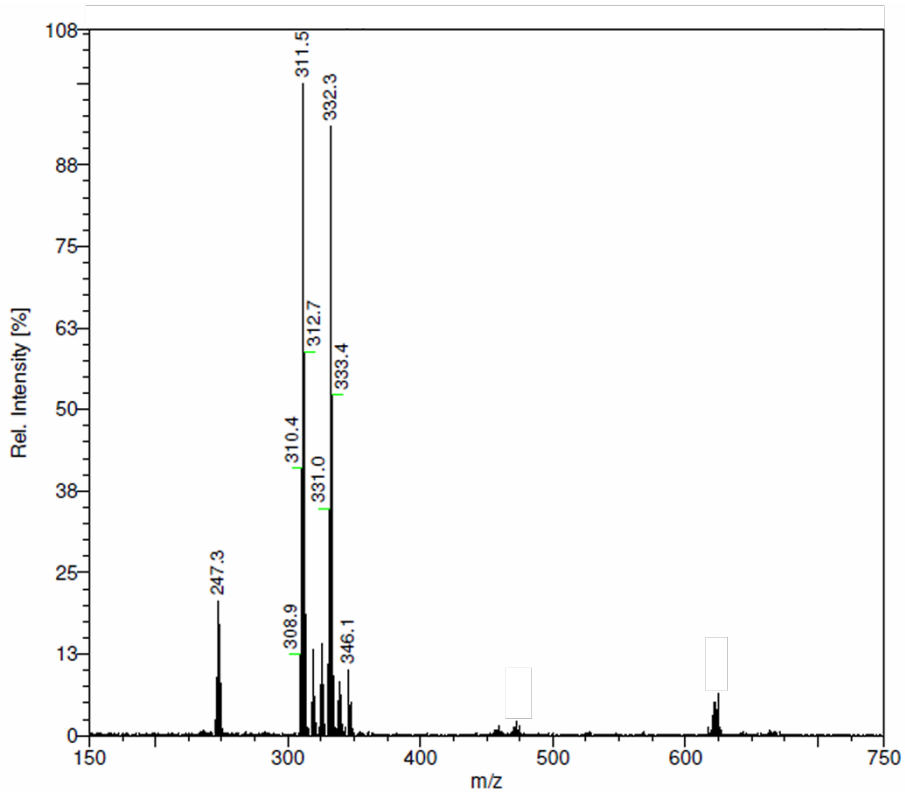

Figure S13. Mass spectrum taken in acetonitrile after 5 min of photolysis of an aqueous solution of [3](PF$_6$)$_2$ under N$_2$ at 298 K showing peaks corresponding to [Ru(bpy)$_2$(CH$_3$CN)$_2$]$^{2+}$ (calcd. m/z = 248.0), [Ru(bpy)$_2$(6)]$^{2+}$ (calcd. m/z = 312.0), [Ru(bpy)$_2$(6)(CH$_3$CN)]$^{2+}$ (calcd. m/z = 332.6), and {[Ru(bpy)$_2$(6)]−H}$^+$ (calcd. m/z = 623.1).

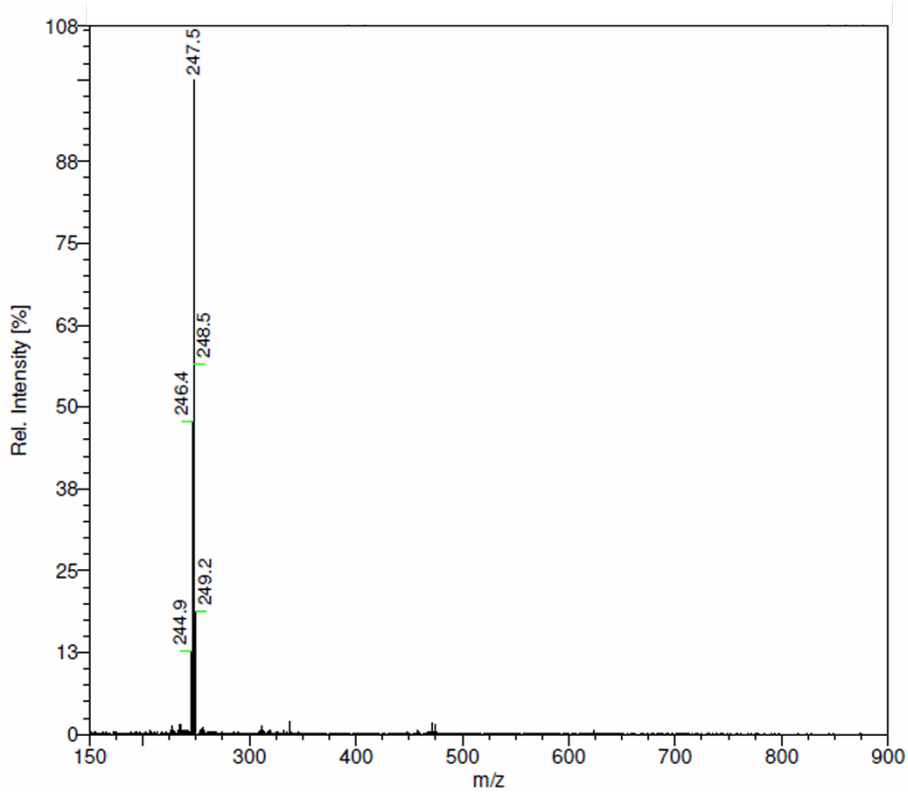

Figure S14. Mass spectrum taken in acetonitrile after 120 min of photolysis of an aqueous solution of [3](PF$_6$)$_2$ under N$_2$ at 298 K showing a peak corresponding to [Ru(bpy)$_2$(CH$_3$CN)$_2$]$^{2+}$ (calcd. m/z = 248.0).

10) Photosubstitution quantum yield measurements: modelling

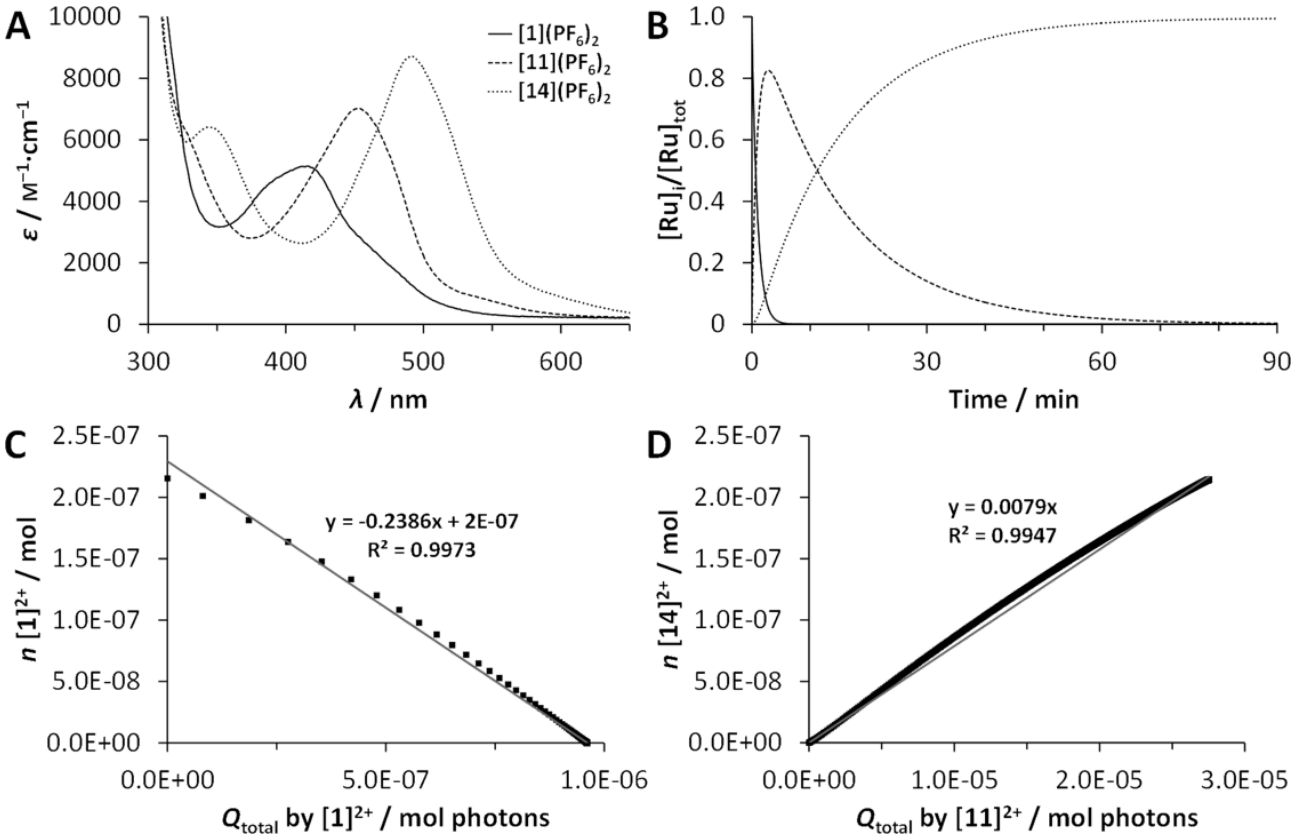

Figure S15. Kinetic data for the two-step photosubstitution (λ = 443 nm, q_p = 2.65 × 10^{-8} mol photons·s^{-1}) of [1](PF$_6$)$_2$ (72 μM) in water under N$_2$ atmosphere at 298 K. (a) Globally fitted UV-Vis absorption spectra of [1]$^{2+}$ (solid line), [11]$^{2+}$ (dashed line), and [14]$^{2+}$ (dotted line) according to fitting using the Glotaran software package. (b) Fitted evolution of the relative concentrations of [1]$^{2+}$ (solid line), [11]$^{2+}$ (dashed line), and [14]$^{2+}$ (dotted line) vs. irradiation time according to global fitting using Glotaran. (c) Plot of the amount of [1]$^{2+}$ (in mol) vs. the total amount of photons absorbed by [1]$^{2+}$ (Q_{total} in mol). The slope of the obtained trend line is the opposite of the photosubstitution quantum yield for the formation of [11]$^{2+}$ from [1]$^{2+}$. (d) Plot of the amount of [14]$^{2+}$ (in mol) vs. the total amount of photons absorbed by [11]$^{2+}$ (Q_{total} in mol). The slope of the obtained trend line is the photosubstitution quantum yield for the formation of [14]$^{2+}$ from [11]$^{2+}$.

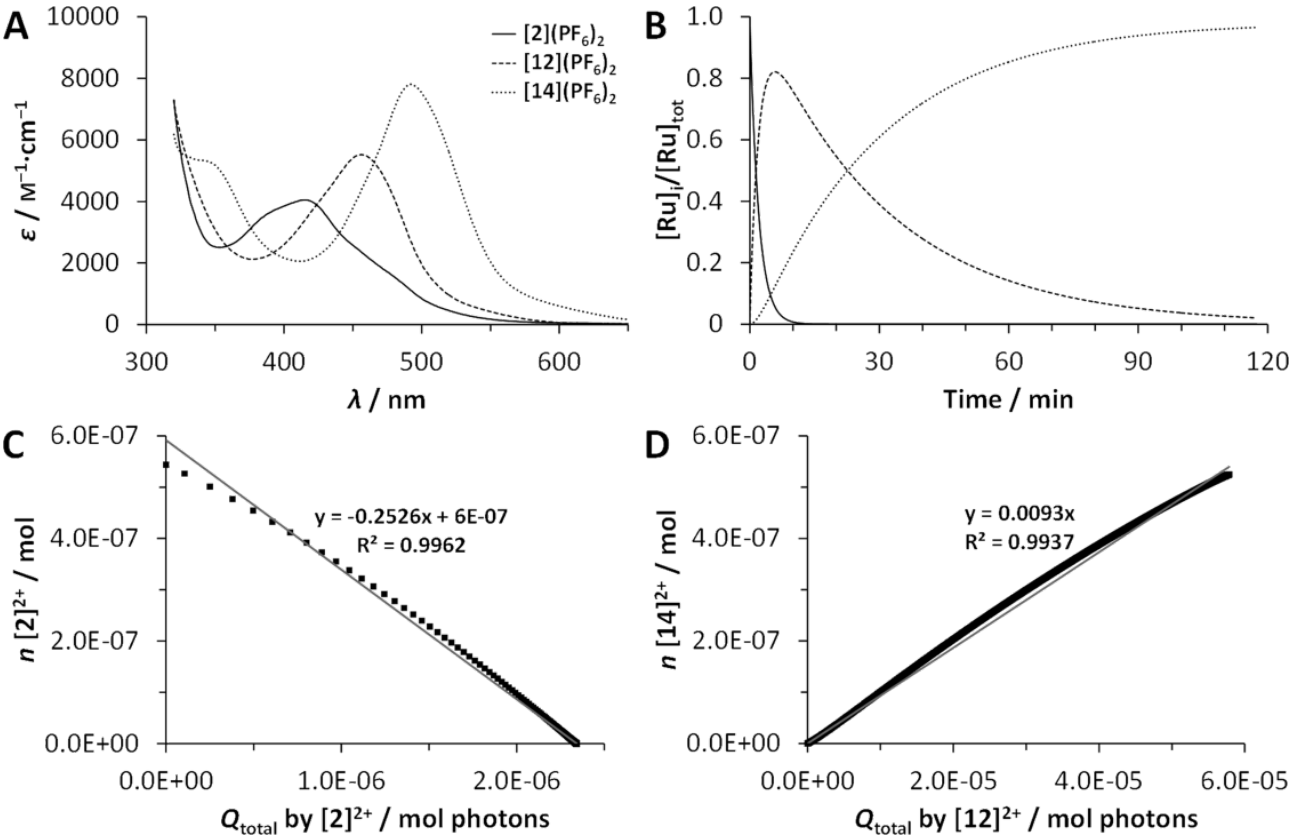

Figure S16. Kinetic data for the two-step photosubstitution (λ = 443 nm, $q_p = 2.85 \times 10^{-8}$ mol photons·s^{-1}) of [2](PF$_6$)$_2$ (181 µM) in water under N$_2$ atmosphere at 298 K. (a) Globally fitted UV-Vis absorption spectra of $[2]^{2+}$ (solid line), $[12]^{2+}$ (dashed line), and $[14]^{2+}$ (dotted line) according to fitting using the Glotaran software package. (b) Fitted evolution of the relative concentrations of $[2]^{2+}$ (solid line), $[12]^{2+}$ (dashed line), and $[14]^{2+}$ (dotted line) vs. irradiation time according to global fitting using Glotaran. (c) Plot of the amount of $[2]^{2+}$ (in mol) vs. the total amount of photons absorbed by $[2]^{2+}$ (Q_{total} in mol). The slope of the obtained trend line is the opposite of the photosubstitution quantum yield for the formation of $[12]^{2+}$ from $[2]^{2+}$. (d) Plot of the amount of $[14]^{2+}$ (in mol) vs. the total amount of photons absorbed by $[12]^{2+}$ (Q_{total} in mol). The slope of the obtained trend line is the photosubstitution quantum yield for the formation of $[14]^{2+}$ from $[12]^{2+}$.

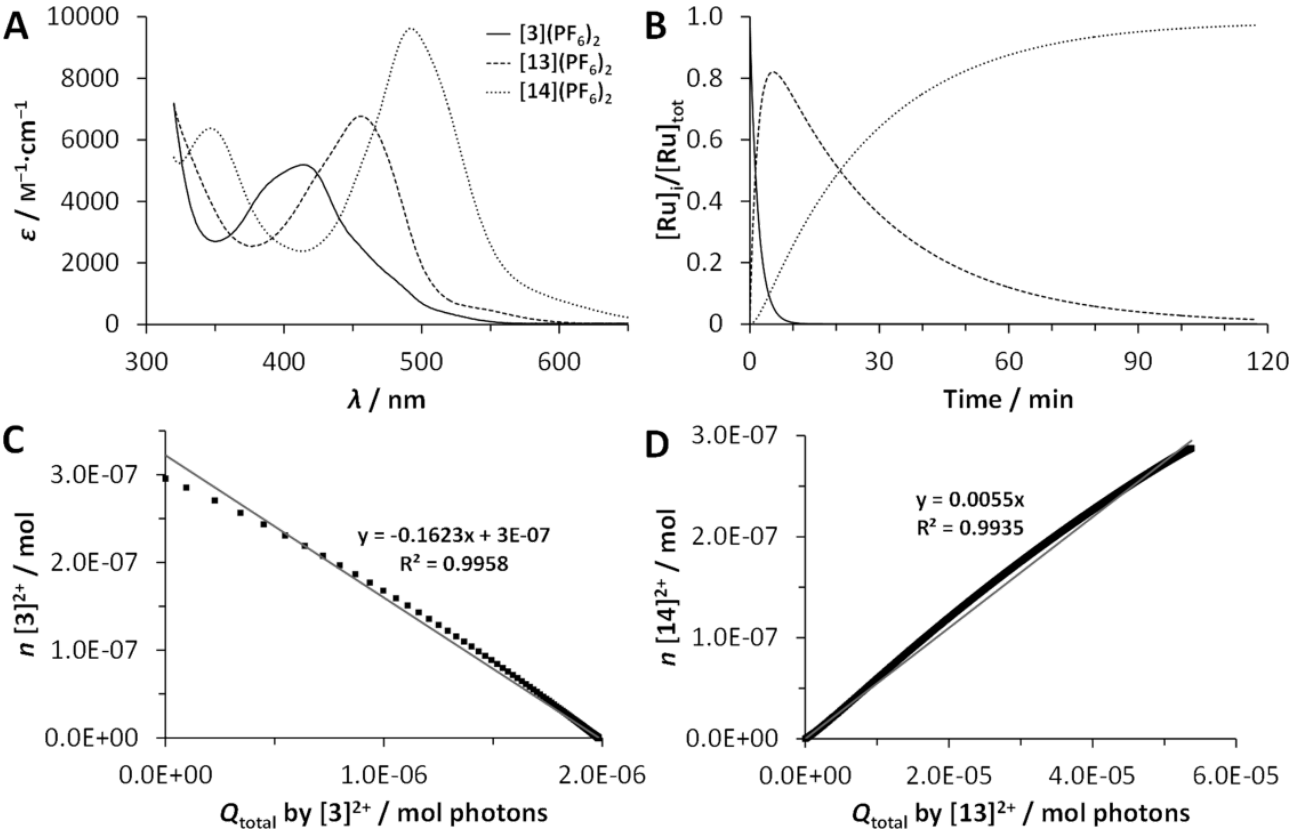

Figure S17. Kinetic data for the two-step photosubstitution (λ = 443 nm, $q_p = 2.85 \times 10^{-8}$ mol photons·s^{-1}) of [3](PF$_6$)$_2$ (99 µM) in water under N$_2$ atmosphere at 298 K. (a) Globally fitted UV-Vis absorption spectra of $[3]^{2+}$ (solid line), $[13]^{2+}$ (dashed line), and $[14]^{2+}$ (dotted line) according to fitting using the Glotaran software package. (b) Fitted evolution of the relative concentrations of $[3]^{2+}$ (solid line), $[13]^{2+}$ (dashed line), and $[14]^{2+}$ (dotted line) vs. irradiation time according to global fitting using Glotaran. (c) Plot of the amount of $[3]^{2+}$ (in mol) vs. the total amount of photons absorbed by $[3]^{2+}$ (Q_{total} in mol). The slope of the obtained trend line is the opposite of the photosubstitution quantum yield for the formation of $[13]^{2+}$ from $[3]^{2+}$. (d) Plot of the amount of $[14]^{2+}$ (in mol) vs. the total amount of photons absorbed by $[13]^{2+}$ (Q_{total} in mol). The slope of the obtained trend line is the photosubstitution quantum yield for the formation of $[14]^{2+}$ from $[13]^{2+}$.

11) 1D NMR of synthesized compounds

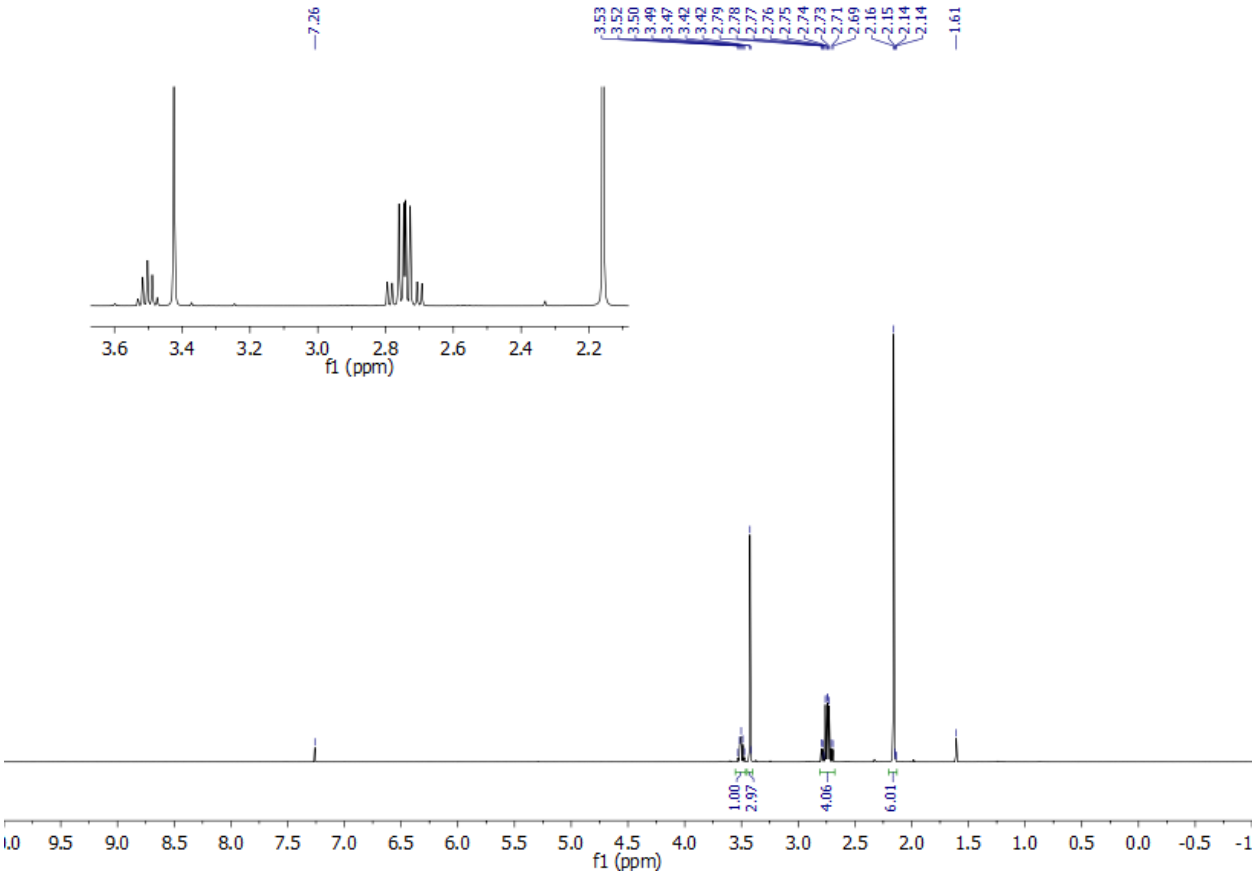

Figure S18. ^{1}H NMR spectrum of compound 5 in $CDCl_3$.

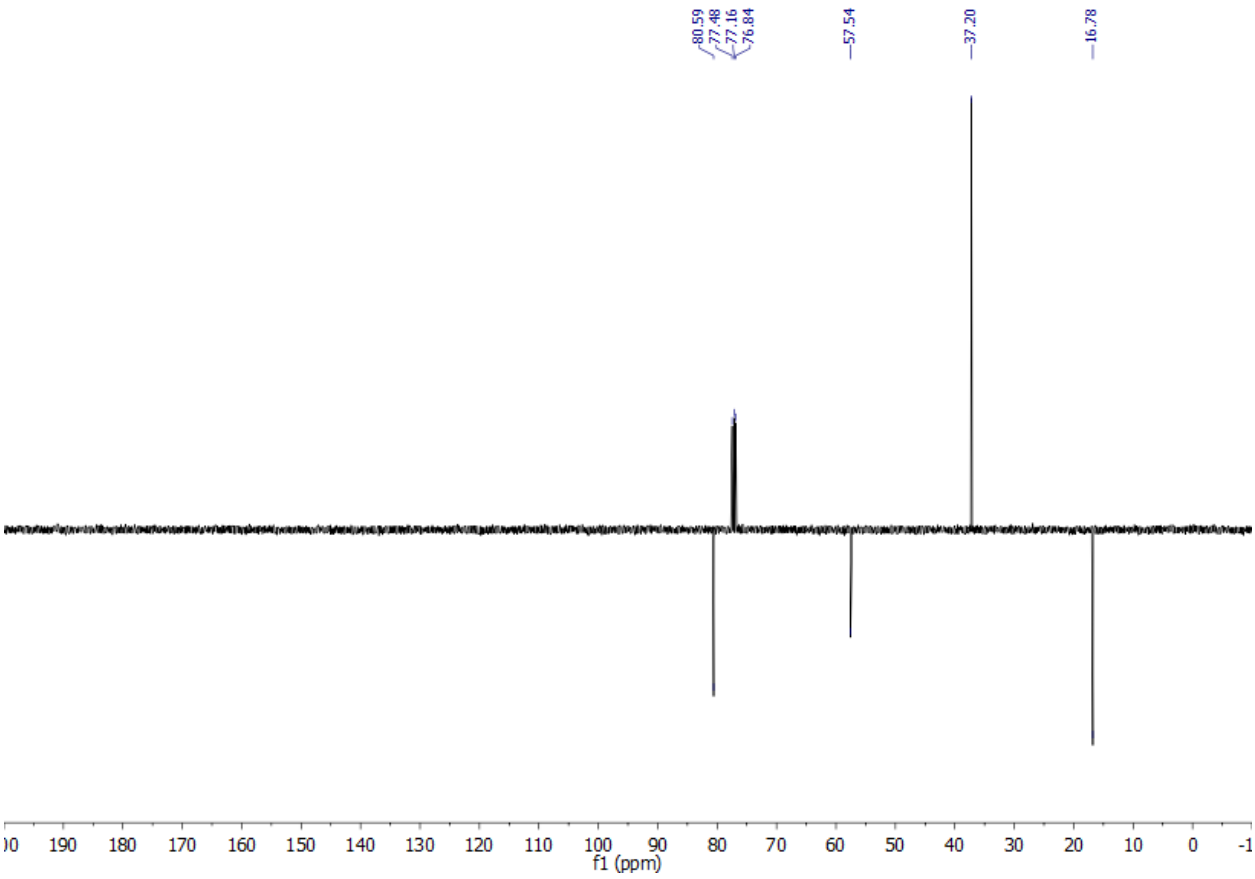

Figure S19. ^{13}C-APT NMR spectrum of compound 5 in $CDCl_3$.

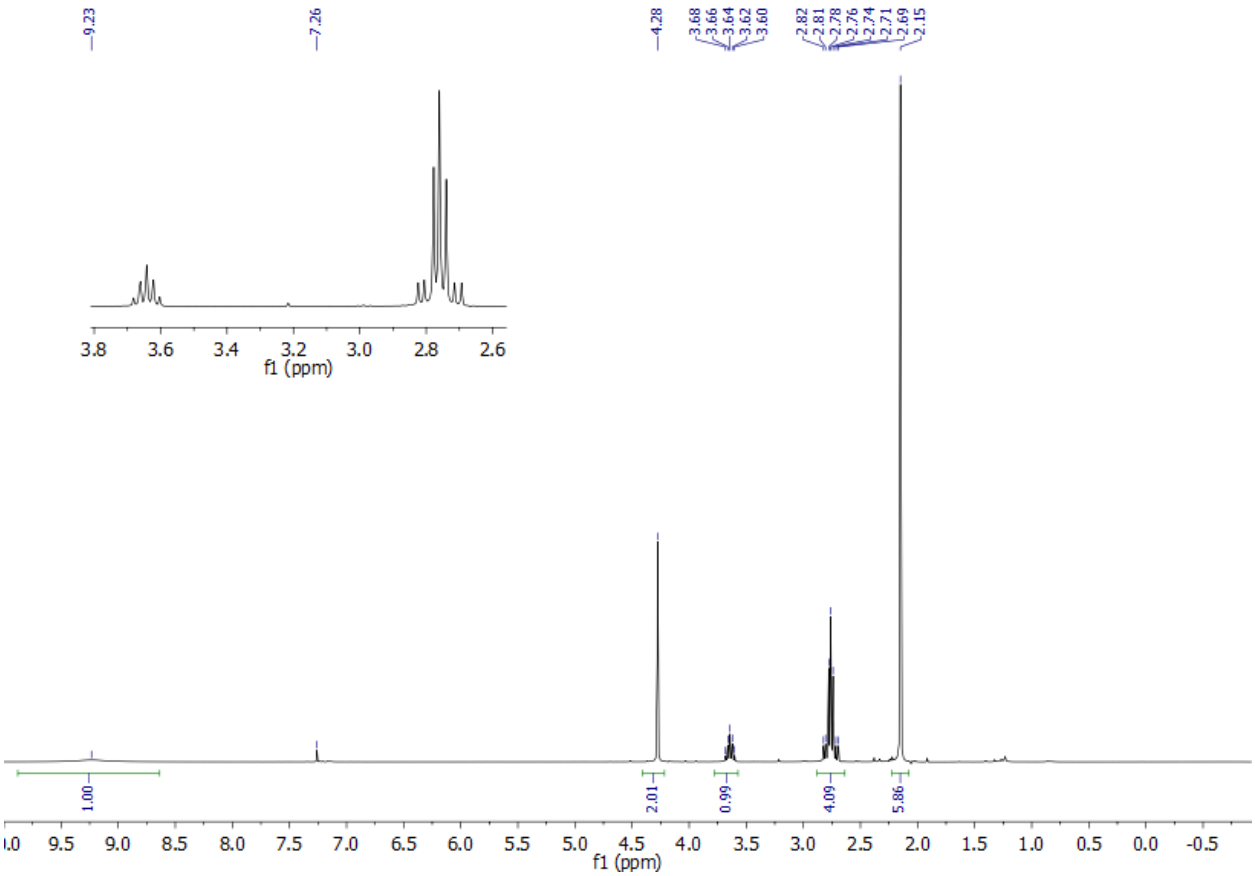

Figure S20. ^{1}H NMR spectrum of compound 6 in $CDCl_3$.

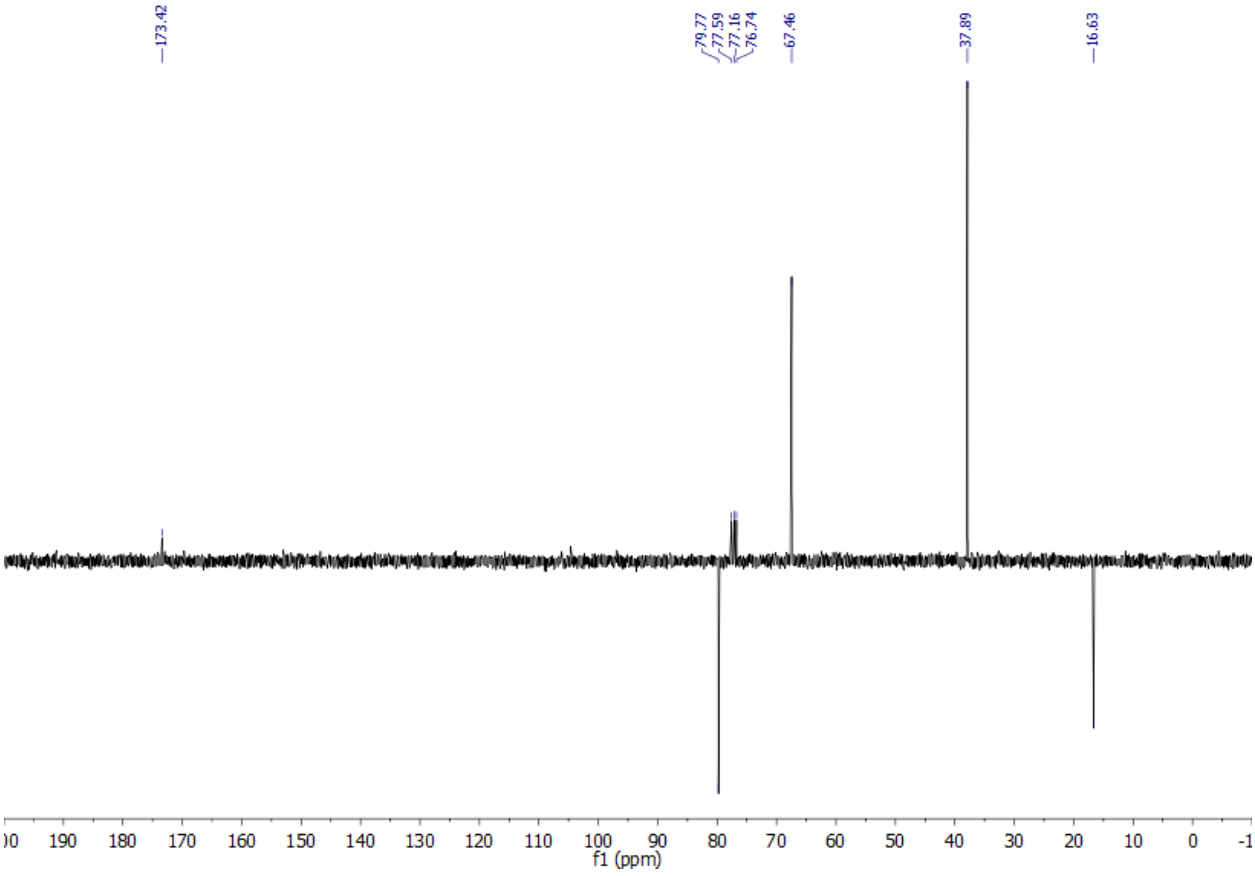

Figure S21. ^{13}C-APT NMR spectrum of compound 6 in $CDCl_3$.

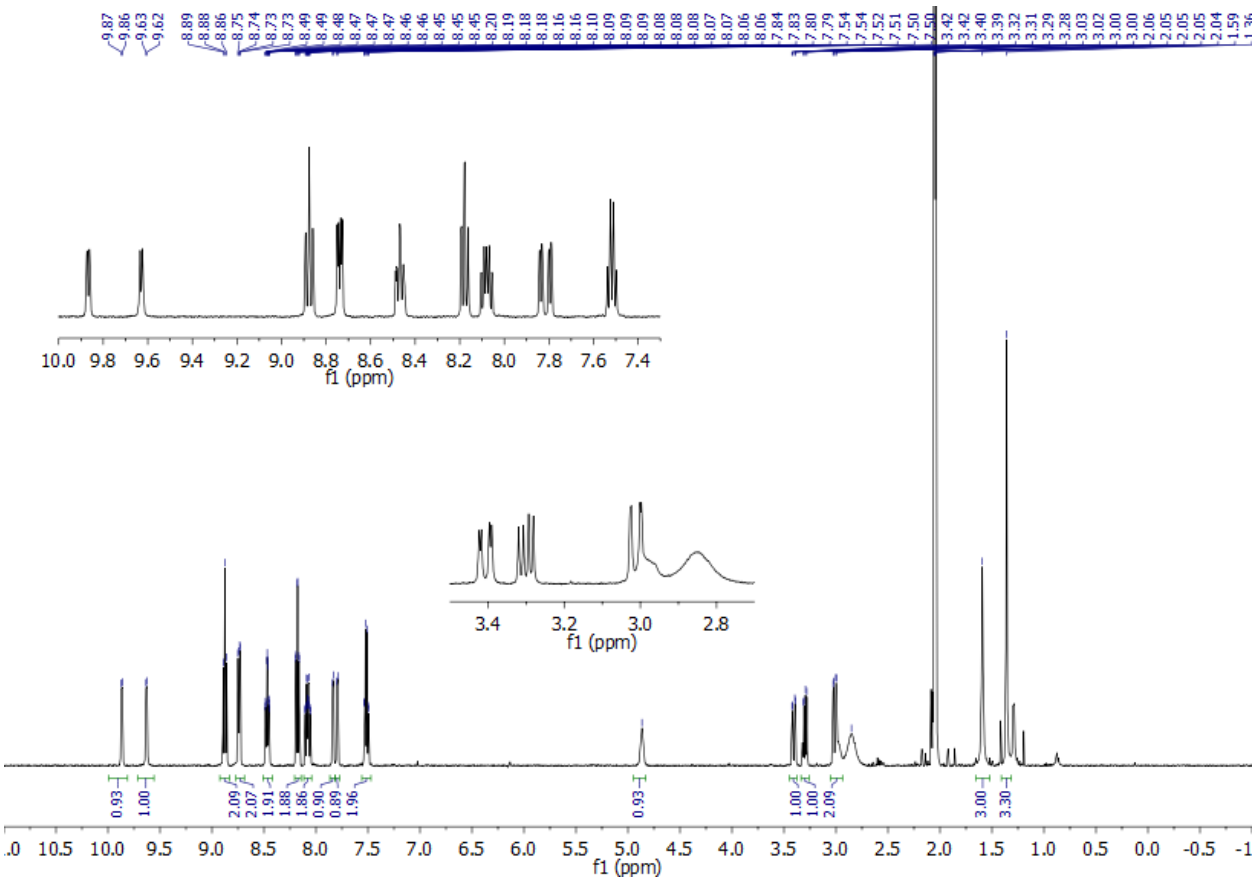

Figure S22. ^{1}H NMR spectrum of compound [1](PF$_6$)$_2$ in acetone-*d6*.

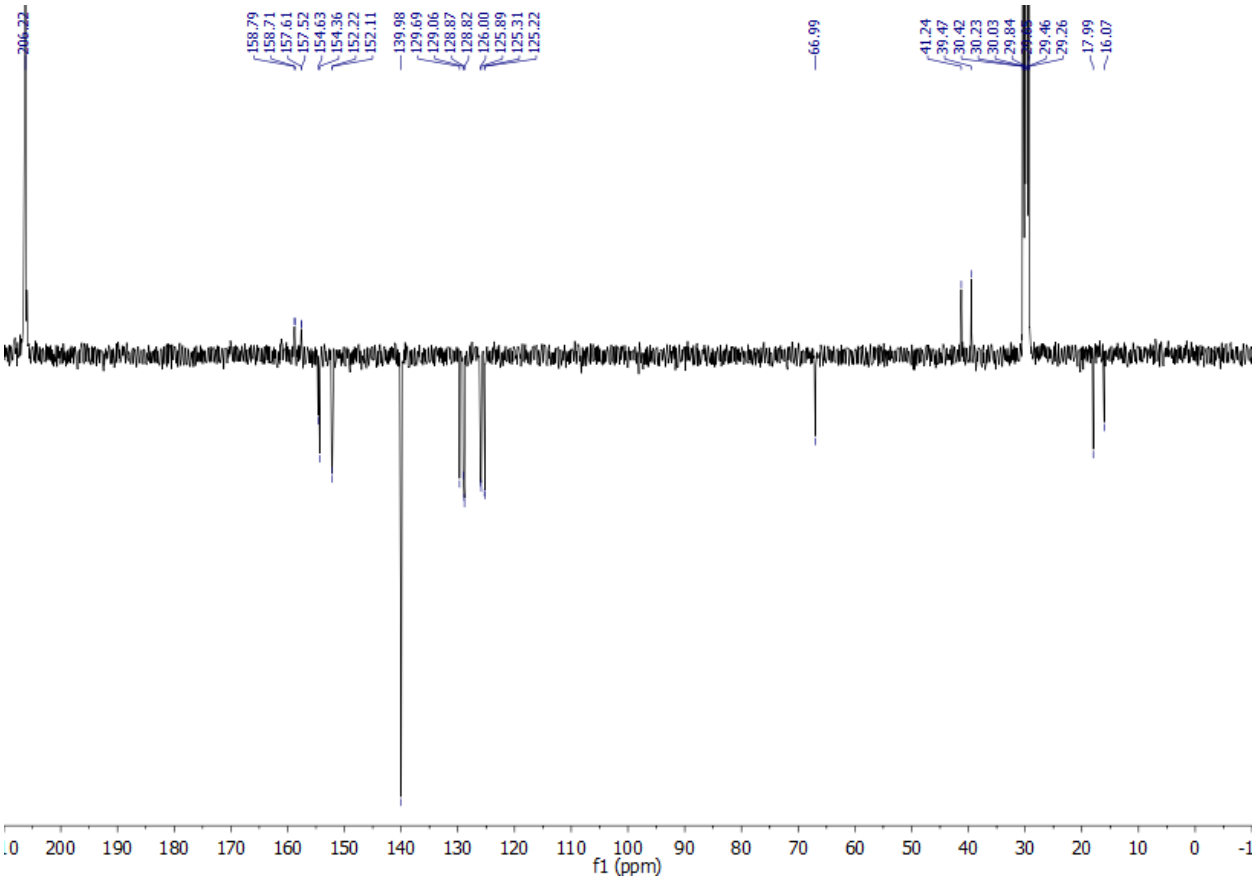

Figure S23. ^{13}C-APT NMR spectrum of compound [1](PF$_6$)$_2$ in acetone-*d6*.

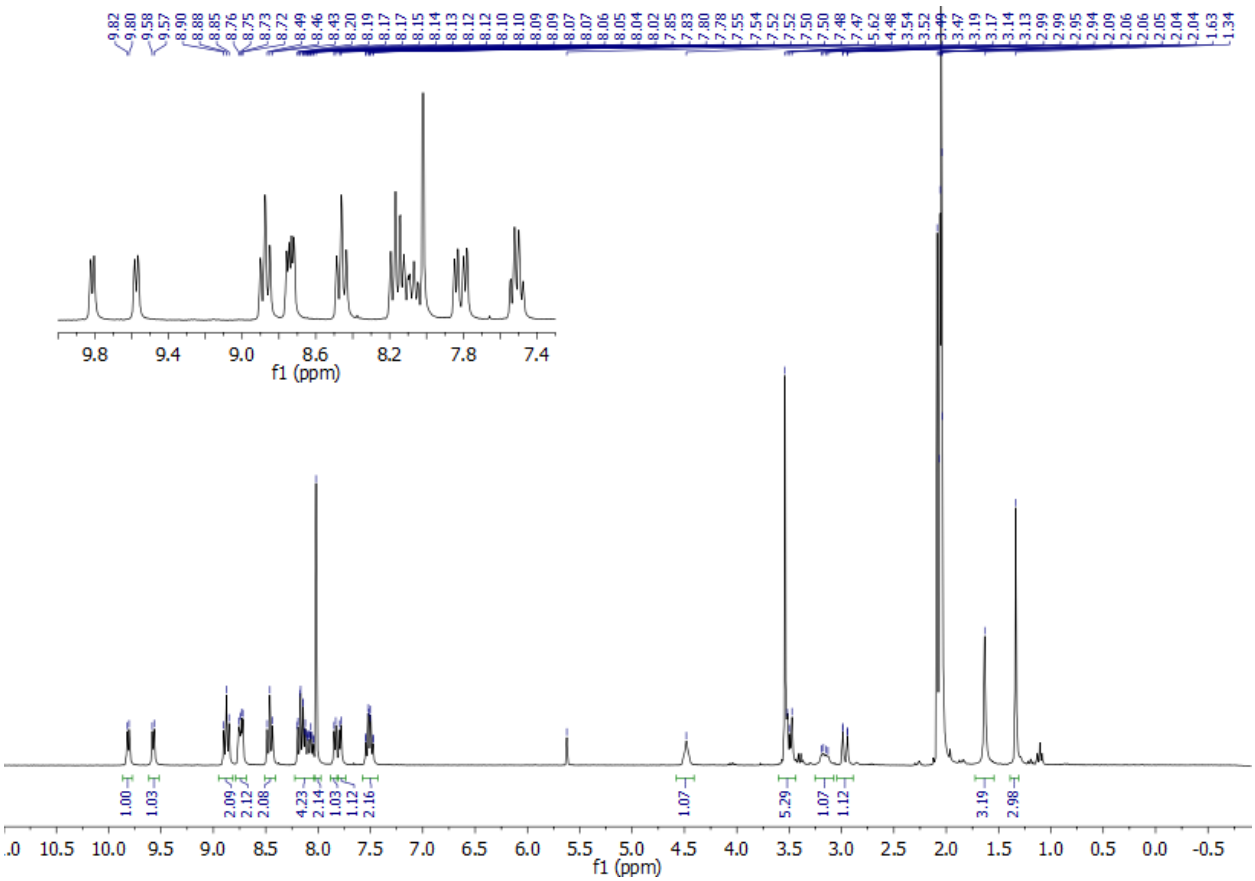

Figure S24. ^{1}H NMR spectrum of compound [2](PF$_6$)$_2$ in acetone-*d6*.

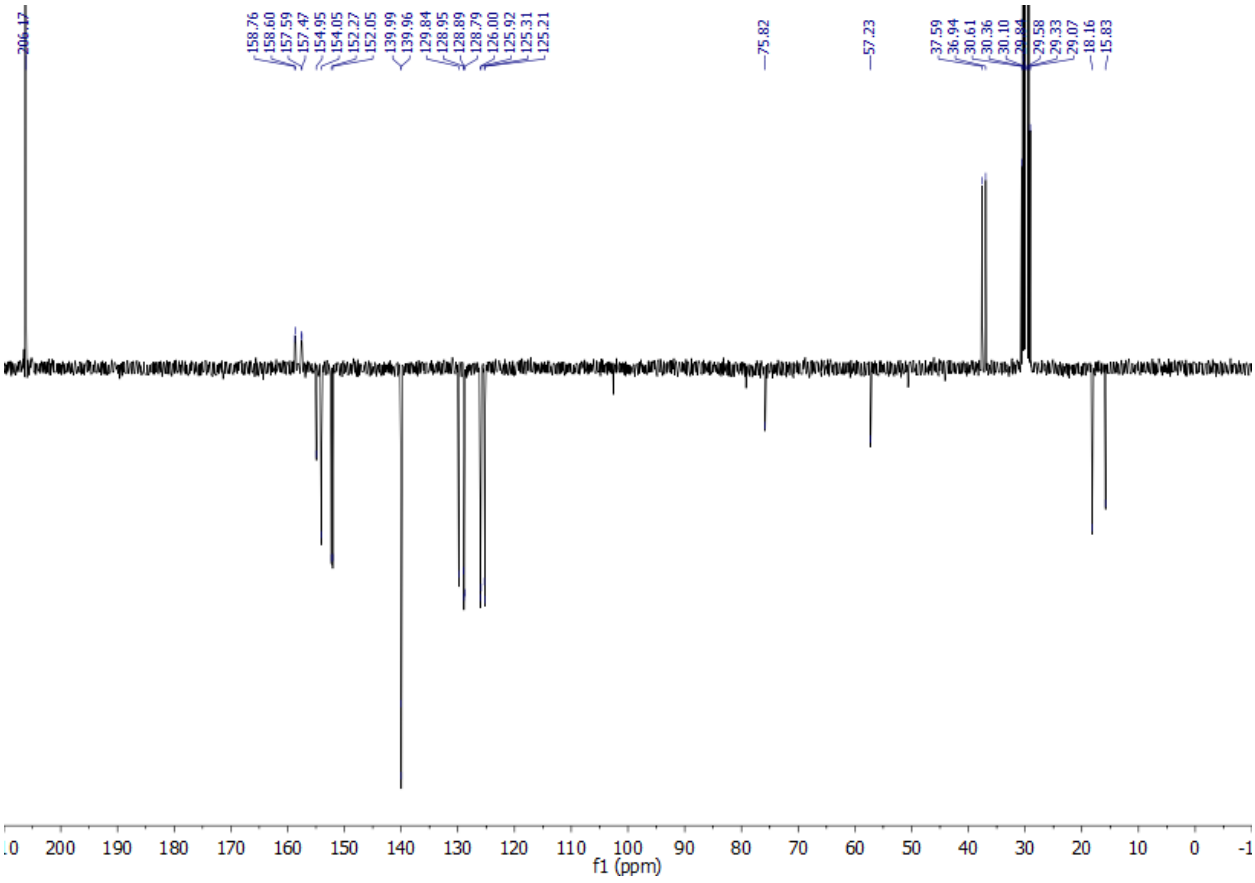

Figure S25. ^{13}C-APT NMR spectrum of compound [2](PF$_6$)$_2$ in acetone-*d6*.

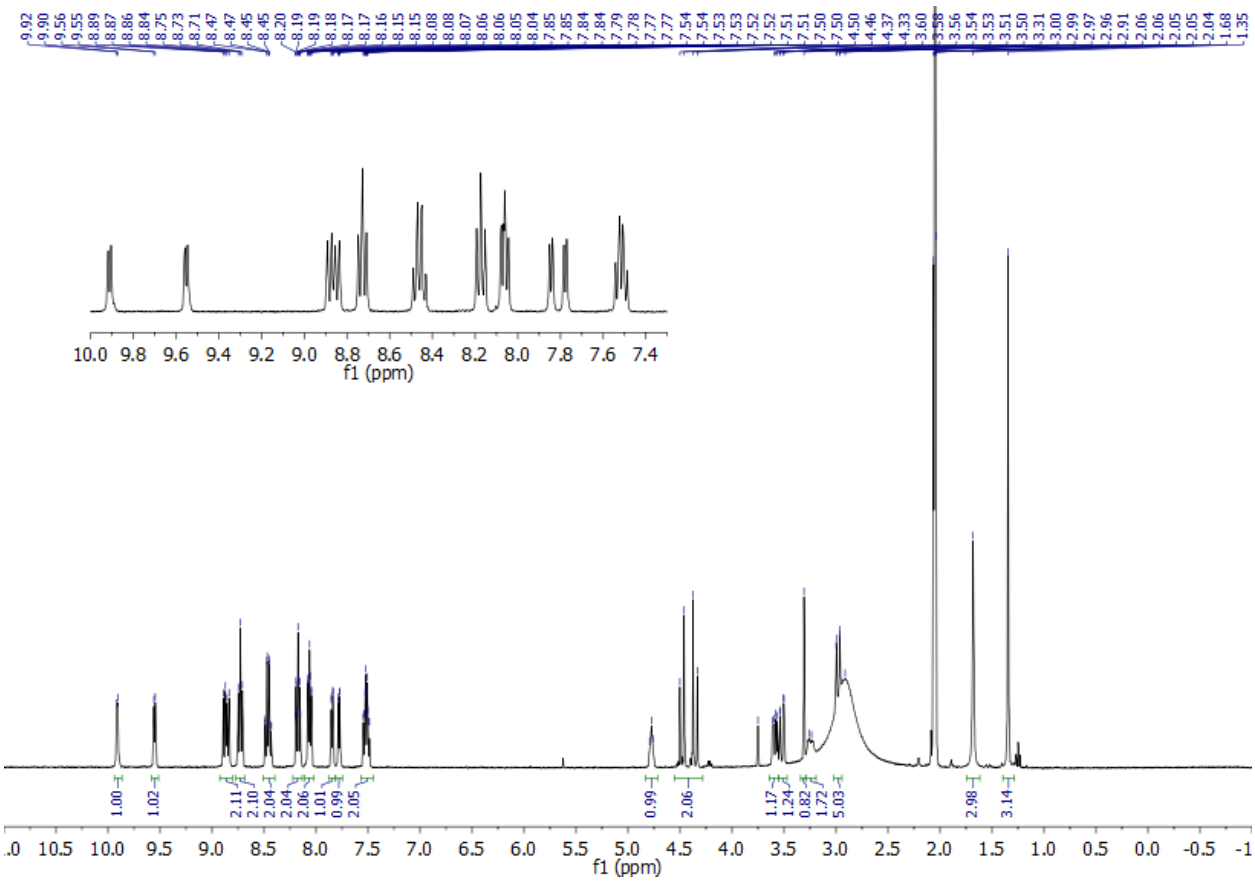

Figure S26. ^{1}H NMR spectrum of compound [3](PF$_6$)$_2$ in acetone-*d6*.

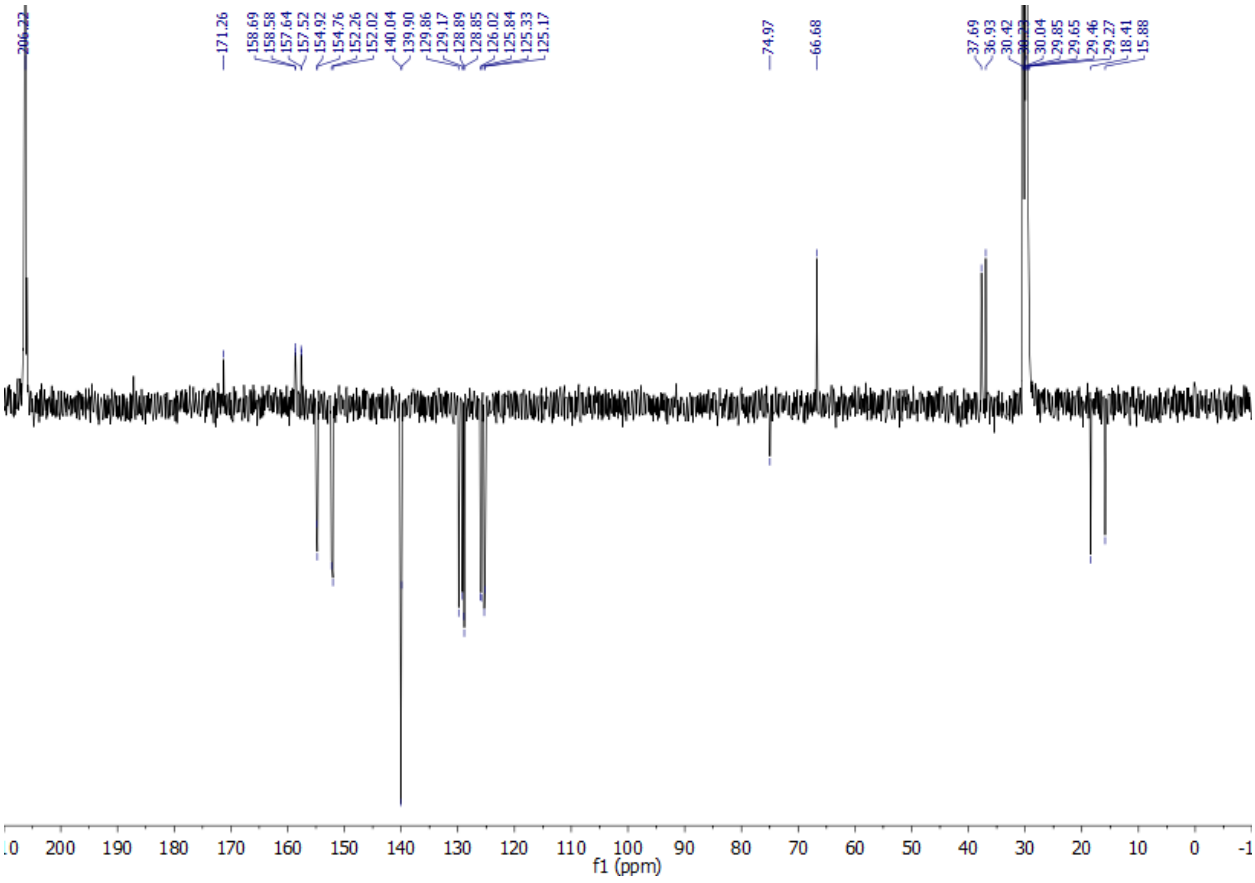

Figure S27. ^{13}C-APT NMR spectrum of compound [3](PF$_6$)$_2$ in acetone-*d6*.

12) References

1. Bahreman, A.; Cuello-Garibo, J.-A.; Bonnet, S. Yellow-light sensitization of a ligand photosubstitution reaction in a ruthenium polypyridyl complex covalently bound to a rhodamine dye. *Dalton Trans.* **2014,** *43*, 4494-4505.
2. Snellenburg, J. J.; Laptenok, S.; Seger, R.; Mullen, K. M.; van Stokkum, I. H. M. Glotaran: A Java-Based Graphical User Interface for the R Package TIMP. *J. Stat. Soft.* **2012,** *49*, 22.
3. DeRosa, M. C.; Crutchley, R. J. Photosensitized singlet oxygen and its applications. *Coord. Chem. Rev.* **2002,** *233*, 351-371.
4. Garcìa-Fresnadillo, D.; Georgiadou, Y.; Orellana, G.; Braun, A. M.; Oliveros, E. Singlet-Oxygen (1Δg) Production by Ruthenium(II) complexes containing polyazaheterocyclic ligands in methanol and in water. *Helv. Chim. Acta* **1996,** *79*, 1222-1238.
5. Suzuki, K.; Kobayashi, A.; Kaneko, S.; Takehira, K.; Yoshihara, T.; Ishida, H.; Shiina, Y.; Oishi, S.; Tobita, S. Reevaluation of absolute luminescence quantum yields of standard solutions using a spectrometer with an integrating sphere and a back-thinned CCD detector. *Phys. Chem. Chem. Phys.* **2009,** *11*, 9850-9860.